ABSTRACT

Title of Document: ACOUSTIC EMISSION-BASED STRUCTURAL HEALTH MANAGEMENT AND PROGNOSTICS SUBJECT TO SMALL FATIGUE CRACKS

Azadeh Keshtgar, Ph.D., 2013

Directed By: Professor Mohammad Modarres, Department of Mechanical Engineering

One of the major concerns in structural health management (SHM) is the early detection of growing crack. Using this, future consequential damage due to crack propagation can be reduced or eliminated by scheduling maintenance which can prevent costly downtime. Early crack detection can also be used to predict the remaining useful life of a system. Acoustic Emission (AE) is a non-destructive testing (NDT) method with potential applications for locating and monitoring fatigue cracks during SHM and prognosis. The research presented in this dissertation focuses on the

structural health monitoring using AE. In this research a correlation between AE signal characteristics and crack growth behavior is established, and a probabilistic model of fatigue crack length distribution based on certain AE signal features is developed. In order to establish the AE signal feature versus the fatigue crack growth model and study the consistency and accuracy of the model, several standard fatigue experiments have been performed using standard test specimens subjected to cyclic loading with different amplitude and frequencies. Bayesian analysis inference is used to estimate the parameters of the model and associated model error. The results indicate that the modified AE crack growth model could be used to predict the crack growth rate distribution at different test conditions.

In the second phase of this research, an AE signal analysis approach was proposed in order to detect the time of crack initiation and assess small crack lengths, which happen during the early stages of damage accumulation. Experimental investigation from uniform cyclic loading tests indicated that initiation of crack could be identified through the statistical analysis of AE signals. A probabilistic AE-based model was developed and the uncertainties of the model were assessed. In addition, a probabilistic model validation approach was implemented to validate the results. The developed models were properly validated and the results were accurate. It was shown that the updated model can be used for detection of crack initiation as well as prediction of small crack growth in early stages of propagation. It was found that the novel AE monitoring technique facilitates early detection of fatigue crack, allows for the original life predictions to be updated and helps to extend the service life of the structure.

Finally, a quantification framework was proposed to evaluate probability of failure of structural integrity using the observed initial crack length. The outcome of this research can be used to assess the reliability of structural health by estimating the probability density function of the length of a detected crack and quantifying the probability of failure at a specified number of cycles. The proposed method has applications in on-line monitoring and evaluation of structural health and shows promise for use in fatigue life assessment.

ACOUSTIC EMISSION-BASED STRUCTURAL HEALTH MANAGEMENT AND PROGNOSTICS SUBJECT TO SMALL FATIGUE CRACKS

By

Azadeh Keshtgar

Dissertation submitted to the Faculty of the Graduate School of the
University of Maryland, College Park, in partial fulfillment
of the requirements for the degree of

Doctor of Philosophy

2013

Advisory Committee:

Professor Mohammad Modarres,(Chair)

Professor Hugh Bruck

Professor Abhijit Dasgupta

Professor Patrick McCluskey

Professor Norman Wereley, (Dean's Representative)

Dedication

To my parents,
who patiently waited for me to pursue my dreams

Acknowledgement

I am especially thankful to my adviser, Prof. Mohammad Modarres for his guidance and supports during each step of this academic endeavor. I also appreciate the guidance and suggestions of the advisory committee: Dr. Dasgupta, Dr. Bruck, Dr. Wereley and Dr. McClusky.

Many thanks are extended to my family, friends and colleagues for their help, support and friendship. I would like to specially acknowledge my friends Victor Ontiveros and Gary Paradee, for all their valuable technical support.

Most importantly, I would like to thank my love of life and best friend, Amir, for giving me new motivations to reach higher. Without his continuous encouragement and support, this achievement would not have been possible.

Table of Contents

List of Tables

List of Figures

List of acronyms

AE: Acoustic Emission

CDF: Cumulative Distribution Function

FORM: First-Order Reliability Method

NDT: Non-Destructive Testing

PDF: Probability Distribution Function

SHM: Structural Health Management

SORM: Second-Order Reliability Method

1 Chapter One: Introduction

1.1 Motivation and background

Structural health management methods have received significant interest in engineering fields that deal with flaw detection, assessment and monitoring of structures during operation. Structures such as bridges and airframes can be subjected to wide range of loading conditions during their operation. Extreme loads may cause initiation of crack and its growth during the life of a component and lead to fatigue failure. Therefore, a prediction system of crack initiation and growth method should be developed to provide guidelines for safe and cost effective inspection intervals. Additionally, this method would ensure that fatigue cracks will not propagate and cause catastrophic failures.

One of the main concerns of fatigue crack propagation is assessment of the crack growth rate to determine how long or how many cycles it takes for a crack to propagate between the initial and critical crack length (Roberts & Talebzadeh, 2003a). By knowing the material crack growth rate characteristics, a cracked structure may be kept in service for an extended amount of time. Traditional fracture mechanics approaches like S-N curves predict the number of cycles to failure, but those approaches are mainly applicable to high-cycle fatigue. They also do not provide crack growth rates and therefore, cannot be used to evaluate the crack severity and remaining useful life of the structure (Parker, 1981).

Despite significant attempts over three decades to establish the application of AE as a useful nondestructive evaluation technique, the determination of crack initiation and prediction of small crack behavior remains a problem. Even though there is no concise and universally accepted definition of the crack length when a crack is initiated, some researchers have tried to investigate the capability of AE to detect crack initiation for different Materials (Bassim & Liu, 1994; Chaswal, Sasikala, Ray, Mannan, & Raj, 2005; Elforjani & Mba, 2009; Marquez & Olivares, 1987; Rahman, Ohba, Yoshioka, & Yamamoto, 2009); but the determination of crack initiation and prediction of small crack behavior remain a problem. Furthermore, the correlation of AE signals with small crack lengths is yet to be fully formulated.

1.2 Research objective

The main objectives of this dissertation are listed as:

1. To review the probabilistic approaches to fatigue crack growth based on AE monitoring capabilities.
2. To demonstrate a novel AE-based methodology to SHM based on very short cracks
3. To updates AE-based crack growth model uncertainty by considering different loading conditions.
4. To demonstrate an NDT approach to detection of crack initiation.
5. To assess the uncertainty about the crack length distribution when initiated using the Bayesian updating approach.

6. To develop a fatigue model based on the correlation between AE signal features and small crack growth.
7. To quantify the probability of remaining life to make a more risk-informed decision.

1.3 Methodology

Mechanical structures typically operate under a wide range of loading scenarios. Different loading features such as frequency and loading ratio can affect model predictions, and this can be verified through specially designed experimental data. The previously proposed fatigue life models based on AE signal features reported by (Talebzadeh & Roberts, 2001), (Biancolini, Brutti, Paparo, & Zanini, 2006) and (Rabiei & Modarres, 2013) have not been validated with respect to different loading conditions. The first step in this research is to study possible effects of cyclic loading features on the AE-based fatigue crack growth rate model by Rabiei and Modarres (2013). This part of research has addressed model development and validation, with respect to changes in loading frequency and loading ratio, through statistical analysis of fatigue data obtained from several AE-based fatigue experiments. In order to establish the AE signal feature versus the fatigue crack growth and study the consistency and variability of the model, several standard fatigue experiments have been conducted using Compact Tension test specimens subjected to cyclic loading with varied loading ratios and frequencies. A Bayesian analysis interface was used to estimate the parameters of the model and associated error term. The results show that the developed AE crack growth model could be used to predict the crack growth rate

distribution at different stress conditions. The outcome of this part is a probabilistic model that includes uncertainties and correlates crack growth rates and AE features.

Previous AE-based crack growth study by Rabiei (Rabiei, 2011) has primarily focused on steady state crack growth with particular interest to correlate the large crack growth rates to AE signals in stable crack growth area (Region II of crack growth curve, see **Error! Reference source not found.**). This model estimates the rate of crack growth when the crack is already in the second region of propagation and the length of crack is large. Thus, the previous research is not able to give an early detection of crack growth. This research focuses on in-situ monitoring of structural health specifically detection of small crack growth and crack initiation using AE technology. The application of AE techniques to detection of crack initiation is explored and the correlation of AE signals with small crack growth rates is investigated. As a result a probabilistic model is developed based on AE signal features of cracks in order to estimate the small crack lengths. The uncertainties of the model are evaluated and a probabilistic model validation is implemented. The methodology proposed in this study could potentially be used for on-line monitoring of fatigue and early detection of damage in aging structures.

Finally, a methodology is proposed to use the outcome of developed AE model for small crack for to calculate failure probability and to evaluate the reliability of fatigue loaded structures. The details of probability theories such as first/second order reliability methods (FORM/SORM) are outlined in the appendix. These techniques are two of the methods utilizing the reliability index. The proposed methodology can be used for estimation of the remaining useful life.

The developed method has significant potential to be used in on-line monitoring and evaluation of structural health and shows promise for use in structures fatigue life. Figure 1-1 illustrates an overview of the proposed methodology and shows that post-processing of captured data in conjunction with model error estimation results in establishing a probabilistic AE-based model. The developed model can be used for detection of crack initiation as well as assessment of small crack growth behavior. This method can be used to assess the reliability of structures and evaluate health by estimating the probability of structure failure at a specified number of cycles, including associated uncertainties.

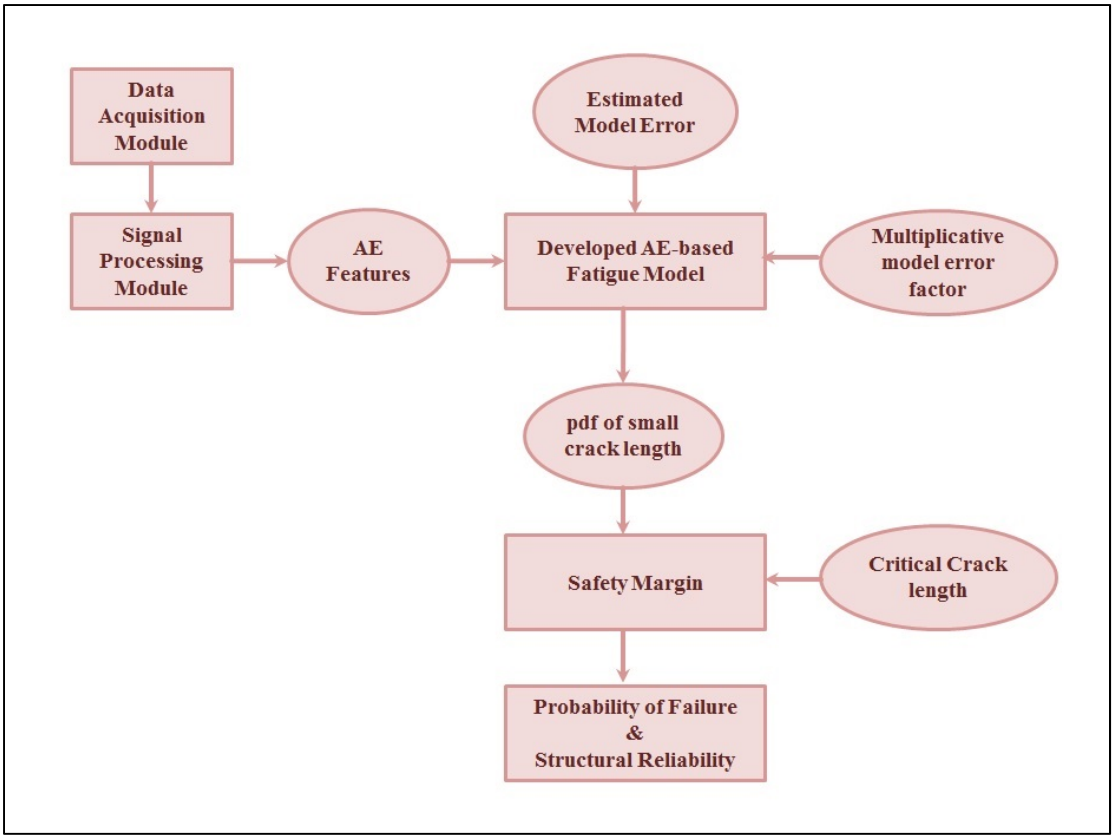

Figure 1-1. Methodology Overview

1.4 Outline of the Dissertation

The rest of this dissertation is organized into four chapters.

Chapter 2 presents a literature review of the history and the theory of AE crack monitoring. Then, Chapters 3 and 4 address the experimental and analytical approaches on AE-based crack growth study. Chapter 3 covers the statistical model development of steady state crack growth for large crack lengths and describes the Bayesian analysis interface used for model development in details. Then Chapter 4 develops a statistical data analysis approach for using AE monitoring to detect crack initiation and develops a probabilistic AE model of small crack growth. The uncertainty analysis and model validation are discussed in this chapter as well. Finally, the conclusions of this dissertation as well as its contributions are listed in Chapters 5. Suggestions for future research are also provided in Chapter 5.

2 Chapter Two: Literature Review

2.1 Fatigue crack growth

2.1.1 Technical background

In materials science, fatigue cracking occurs when a material is subjected to cyclic loading. When the cyclic load is above a certain threshold, a microscopic crack will start to form at the stress concentrated locations. The crack will be growing and reached a critical threshold, and then a sudden fracture takes place in the structure. From an engineering perspective, the American Society of Testing Material (ASTM) defines fatigue as: "the process of progressive localized permanent structural change occurring in a material subjected to conditions which produce fluctuating stresses and strains at some point or points and which may culminate in cracks or complete fracture after a sufficient number of fluctuations"(Fuchs & Stephen, 1980). It has been very challenging to assess the loss of structure integrity due to fatigue cracking in variety of aging structure such as airframes, piping, bridges, offshore structures and power plans in order to prevent fatigue related failures.

Analysis of crack growth behavior is usually based on the relationship between crack growth rate (da/dN) and stress intensity range (ΔK). **Error! Reference source not found.** shows a schematic plot of the typical relationship between da/dN and ΔK. Basically the graph can be divided into three regions. The first region is called the threshold region that is associated with small growth of cracks just after cracks are initiated. This region represents the early development of fatigue crack and small crack growth rates. The second region is the stable crack growth region. In this

region, the slope of the *log(da/dN)* versus *log(ΔK)* curve is approximately linear. In practice, Paris law (Paris & Erdogan, 1963) is calibrated to model this linear interval. The third region is unstable crack growth toward rapid fracture (Bannantine, Comer, & Handrock, 1989).

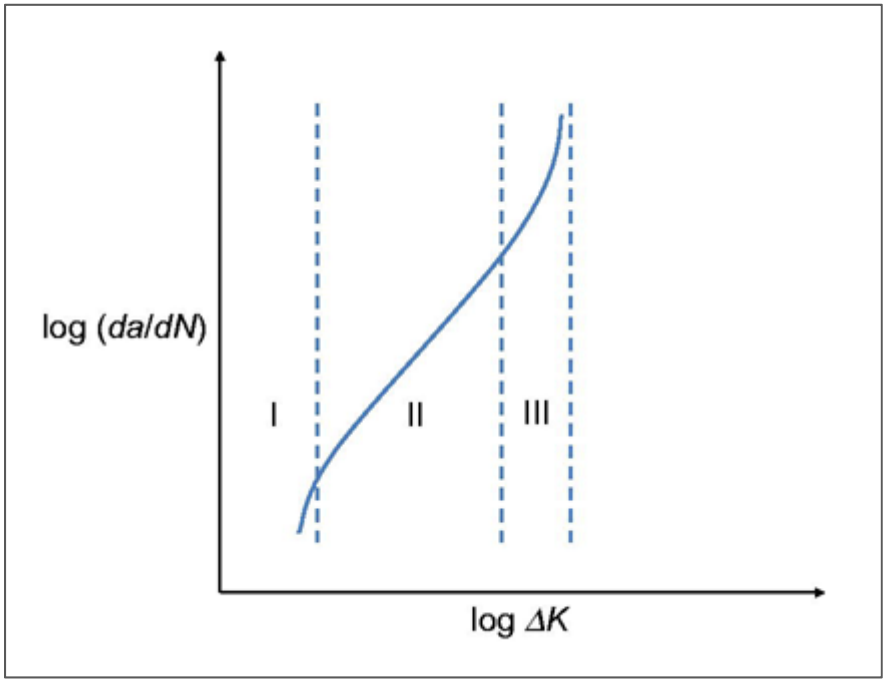

Figure 2-1 Schematic of crack growth rate versus stress intensity factor curve

2.1.2 Small crack growth and crack initiation

One of the challenging problems in a study of fracture mechanics is the detection of crack initiation, as well as prediction of small crack growth rates, in early stages of propagation. Although the behavior of small cracks is an extremely complicated subject, the importance of small crack detection in health monitoring of structures cannot be ignored. This complexity is mainly due to variety of microstructures used

in structural materials, in addition to the variety of parameters affecting crack in its formation and early stages of growing (ASTM, 1994). Many researchers have worked on small cracks, and there are various published small-crack data in the literature, as well as different models to simulate the small crack growth behavior (Forth, Newman, & Forman, 2005; Künkler et al., 2008; Marder, 1989; McDowell, 1997; Shyam, Allison, & Jones, 2005).

Available fatigue growth prediction models usually require a known existing flaw length and may be challenging to apply to crack initiation period. The crack initiation phase generally corresponds to formation and growth of short cracks (Bhattacharya & Ellingwood, 1998), but the threshold crack length at which initiation happens lacks a universally accepted definition. Kujawski (Kujawski & Ellyin, 1992) highlighted the point with this comment:

"There is still some difficulty with the terminology when referring to the crack initiation and propagation stages. Although no absolute boundaries between these stages have been defined, usually the crack initiation is associated with an arbitrarily specified crack length. A crack length ranging from a size of grain diameter to about 50 to 100 μm is used depending on material and scale of interest". However an extensive choice of values have been used of structures for length of crack initiation in the literature, for example 51 μm for carbon steel; 120 μm for BS250A53 steel and 1 mm for En7A steel. (Bhattacharya & Ellingwood, 1998), up to 500 μm for aluminum (Pearson, 1975). US Navy defines the presence of a crack 250 μm in length, as the crack initiation (Iyyer, Sarkar, Merrill, & Phan, 2007). In this research the crack length of 50 μm is used as the crack initiation for Al7075-T6.

2.2 Acoustic Emission background

2.2.1 Basic Theory

Acoustic Emission (AE) is defined as a transient elastic wave generated by the rapid release of energy within a material and an AE signal is the electrical signal produced by a sensor in response to this wave (Beattie, 1983; Berkovits & Fang, 1995).

There is a fundamental difference between AE and "ultrasonic" field. The difference is that AE is produced by the material itself, while in ultrasonic acoustic wave is generated by an external source and in presented into the material. In AE testing, the experimentalist does not have control over the sound generation mechanism but can only subject the material to the situation (e.g. cyclic loading) which will cause the generation of AE (e.g. due to fatigue).

Some of the factors that determine the characteristics of the AE signal are the mechanism that generated the emission, the means by which it travels through the material and the sensor that transforms the emission into the signal (Beattie, 1983). The most commonly used AE feature for fatigue is the ring down counts which is defined as the number of times that the AE signal amplitude exceeds a predefined subjective threshold value (Bassim & Liu, 1994; Talebzadeh & Roberts, 2001). There are other features of AE signal such as rise time, energy, and amplitude (Figure 2-2) that can be used to determine signal characteristics. The definition of some AE features can be found in the next section. Some of these AE features, as well as

counts, will be used later in this research in order to detect damage initiation and study small crack growth.

2.2.2 AE Terminology

Acoustic Emission may be defined as a transient elastic wave generated by the rapid release of energy within the material and AE signal is the electrical signal generated by the sensor to response to the wave. The use of AE has been limited primarily to statistical analysis of events. An event is defined as one acoustical waveform. The waveform has traditionally been described in terms of its features. An example of a typical AE waveform and its features is shown in Figure 2-2 for clarity. In addition to recording the number of acoustic events and correlating this number to the level of damage (Eberhardt, Stead, Stimpson, & Read, 1997) , it is also possible to record certain features of the AE waveforms. Some features are defined with respect to the specified threshold limit (Figure 2-2). These waveform features include but not limited to the ones listed below (Beattie, 1983; R. K. Miller, Hill, & Moore, 2005; Physical Acoustic Corporation, 2007):

- Counts: Also known as "ring down count" is defined as the number of times that the AE signal amplitude exceeds a predefined subjective threshold value. In general, large event produce more counts than a small event. This provides a measure of strength of the AE event.
- Amplitude: The AE amplitude is the largest voltage peak in the waveform signal. Peak amplitude usually recorded in log units (decibels) to provide accurate assessment for both large and small AE events.

- Rise Time: The AE rise time is the time elapsed from when the waveform initially crosses the threshold until it reaches its peak. In the other word, it measures the time it takes to reach the peak amplitude.
- Energy: AE energy is the measured area under the rectified signal envelope. To measure energy directly, the waveform signal needs to be digitized and integrated (Analog-to-digital convertor).
- Duration: Is the time elapsed from when the waveform initially crosses the threshold until the waveform drops beneath the threshold again. That means the total time that the waveform amplitude remains above the threshold.

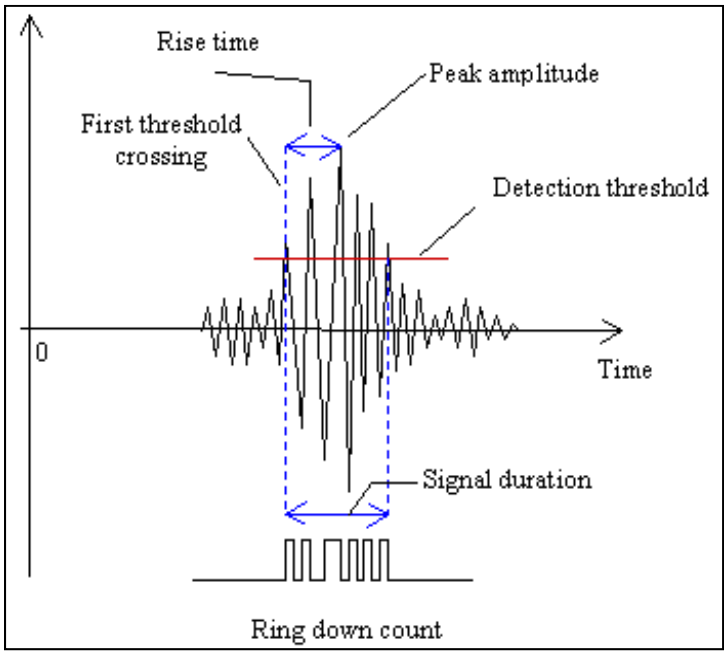

Figure 2-2 Typical AE signal and its characteristics ***(Kappatos & Dermatas, 2007)***

2.3 AE Fatigue Literature

The application of AE as a non-destructive testing (NDT) method has been an active area of research over the past three decades. Acoustic emissions have been used during fatigue crack-propagation tests and growing fatigue cracks have been reported detectable by AE (Bassim & Liu, 1994; Lindley, Palmer, & Richards, 1978). Previous studies have identified the number of AE ring-down counts, as a useful feature of AE signals for measuring crack growth (Berkovits & Fang, 1995; Lindley et al., 1978; Morton, Harrington, & Bjeletich, 1973; Talebzadeh & Roberts, 2001; Wang, Li, Ke, & Zhu, 1992). Measurement of AE counts is one of the easiest and most useful methods of analyzing AE signals. Studies show the relationship between the stress intensity factor range and the number of AE counts, through an equation similar to the Paris-Erdogan equation (Bassim & Liu, 1994; Berkovits & Fang, 1995; Gong, Nyborg, & Oommen, 1992). The AE count rate versus cyclic loading has also been shown (Bassim & Liu, 1994) to follow a power law, much similar to the Paris-Erdogan crack growth rate equation (Paris & Erdogan, 1963). The model was used later by many researchers (Biancolini et al., 2006; Rabiei & Modarres, 2013; Roberts & Talebzadeh, 2003a). It will be discussed with more details in the next section.

Several attempts have been made to relate other AE parameters such as energy and amplitude to material characteristics during fatigue such as stress intensity factor range (ΔK), maximum stress intensity factor (K_{max}) and crack growth rates. Konsztowicz and Fontaine (Konsztowicz & Fontaine, 1989) investigated the correlation of AE amplitude with strength loss after thermal shock in a partially stabilized zirconia. They suggested that high amplitude AE events are due to crack

propagation through the crystalline phase of the ceramic body. It was also shown by experimental results on aluminum, titanium and steel alloys that sum of the stress-wave amplitudes has a relationship with incremental area swept out by the crack (Gerberich & Hartbower, 1967). The experimental research of Harris and Bell (Harris & Bell, 1977) on unflawed tensile tests, pre-cracked stress corrosion cracking, pre-cracked fracture toughness test and fatigue crack growth showed that in the case of unflawed tensile specimens, energy techniques appeared somewhat superior to counts. In all other cases, a direct relationship between counts and energy was obtained. More recent studies such as the research by Kim (Kim, Yoon, Jeong, & Lee, 2004) tested the application of artificial neural networks to predict the stress intensity factor based on AE energy and peak amplitude for a specific type of steel.

Acoustic Emission count rates and the rate of crack propagation have also been proven to be correlated (Berkovits & Fang, 1995; Rabiei & Modarres, 2013; Talebzadeh & Roberts, 2001). All the results from the aforementioned researches agree that as the AE count rate increases, the crack-growth rate increases. Nevertheless, how the increase of the AE count rate is related to that of the crack-growth rate varies with different materials (Berkovits & Fang, 1995; C. S. Lee, Park, & Chang, 1996; Moorthy, Jayakumar, & Raj, 1996; Wang et al., 1992; Williams, DeLonga, & Lee, 1982).

The investigations on aluminum alloys (C. S. Lee et al., 1996),Titanium alloys (Williams et al., 1982) and some steels (C. S. Lee et al., 1996; Wang et al., 1992) indicated that a log-log plot of the AE cumulative counts and crack-growth rate versus stress-intensity-factor range was linear. Based on this finding, a probabilistic

AE-based model has been proposed few years later by Rabiei (Rabiei & Modarres, 2013) which correlates AE count rates with the crack growth rates for Al7075-T6. The model is descried in details in the following section. However, their model (Rabiei & Modarres, 2013) was based on a single experiment and was not validated with respect to different loading conditions. Hence, the first step of current research is to study possible effects of cyclic loading features on this model. Also, above-mentioned model has been proposed for large crack growth in Region *II* of crack growth curve (Figure 2-1) and does not consider the crack growth in early stages of fatigue namely Region *I*. Study of AE-based small crack growth constitutes the second part of the current research.

2.3.1 AE fatigue models for life prediction

As discussed earlier, several researchers attempted to relate AE parameters such as count, energy, amplitude to material characteristics during fatigue such as stress intensity factor range (ΔK), maximum stress intensity factor (K_{max}) and crack growth rates. Studies show the relationship between the stress intensity factor range and the number of AE counts, through an equation similar to the Paris-Erdogan equation (Bassim & Liu, 1994; Gong et al., 1992) . A leading general model that relates the AE count rate to the crack growth rate is proposed by Bianocolini et al. (Biancolini et al., 2006) and Rabiei (Rabiei, 2011) has the form of:

$$\frac{dc}{dN} = \beta_1 \left(\frac{da}{dN} \right)^{\beta_2} \tag{2.1}$$

where c is the AE count, a is crack length, N the number of loading cycles (therefore (da/dN) would be crack growth rate and (dc/dN) would be the AE count rate) and β_1 and β_2 are model parameters. Rabiei (Rabiei, 2011) described the linear regression form of Eq. (1.1) by taking logarithm of both sides of this equation and adding an error term as:

$$\log\left(\frac{da}{dN} \right) = \alpha_1 \log\left(\frac{dc}{dN} \right) + \alpha_2 + \varepsilon \tag{2.2}$$

and

$$\begin{aligned} \varepsilon &\approx N(0, \sigma) \\ \sigma &= \gamma_1 \exp\left(\gamma_2 \frac{dc}{dN} \right) \end{aligned} \tag{2.3}$$

Rabiei suggested that the error term, ε in Eq. (2.2) accounts for difference between the model prediction and the observed AE count rate. The proposed model is shown to be applicable to steady state crack growth region (large crack growth rates). The correlation of AE with small crack growth rates (Region *I*) will be studied later in this research. The model described by Eq. (2.3) assumes that in Region *II* the smaller crack lengths are harder to measure and as the crack becomes larger, the measurement

of crack length becomes more accurate. In order to capture any changes in the error distribution, it was assumed that the error follows a normal probability density function with mean of zero and standard deviation of σ. To capture any dependence on the crack length, Rabiei (Rabiei, 2011) assumed that σ follows a two-parameter exponential distribution and changes as a function of count rates Eq. (2.3). Based on a single experiment Rabiei concluded that σ was independent of crack growth rate (i.e., $\gamma_2 \approx 0$).The significance of this proposed model is that once the model parameters are determined experimentally, this equation can be used to estimate crack growth rates by monitoring AE signals and extracting the count rate parameters from the observed signals.

2.3.2 AE crack initiation literature

The application of AE as a nondestructive testing method for detection of crack initiation has been very limited due to large amount of extraneous noise created during a typical fatigue test set up. The lack of significant AE events in preliminary stages of fatigue testing makes it more challenging to differentiate background noise from fracture-related AE events (Eberhardt et al., 1997). Despite significant number of researches to establish the application of AE in structural fatigue growth studies, the determination of crack initiation and prediction of small crack behavior remains a problem.

Considerable number of researchers have focused on the study of small crack growth behavior and different small-crack test methods (some examples include Forth et al.,

2005; Künkler et al., 2008; McDowell, 1997; Shyam et al., 2005); but no AE-based model for small crack growth have been offered. However, most of the success in correlating AE activities with crack growth has involved the latter stages of crack development (Regions *II* and *III* of the crack growth curve).

Few studies have been carried out to combine fracture toughness experiments with AE techniques in order to detect the damage initiation. In 1987, Marquez and Olivares (Marquez & Olivares, 1987) utilized an AE recording system to determine crack initiation and propagation at a thermally sprayed coating interface of nickel-chrome alloy with substrate of AISI 1045 steel. This study initiated an idea of relating abnormal behavior of AE signals to crack related events.

However, it was not until 2005 that Chaswal (Chaswal et al., 2005) identified that AE amplitude is about an order of magnitude lower in Region *I* than in Region *II* due to lower ΔK values. They investigated how low amplitude bursts in a short duration of time in Region *I* correspond to micro-cleavage in thermally aged steel plates. More recent studies including the research of Rahman (Rahman et al., 2009) and Mba (Elforjani & Mba, 2009) hypothesized that a sudden and significant increase in AE events corresponds to damage initiation. Rahman (Rahman et al., 2009) offered that significant increase in hit count data might correspond to incipient damage due to wear in rolling elements during their contacts. Mba (Elforjani & Mba, 2009) presented result of their experimental investigation for detecting natural crack in slow speed shafts. They believe that the first increase in AE energy can be due to crack initiation, and the large transition of AE energy at the end of the fatigue testing is due to rapid propagation.

Despite a number of studies related to AE-based detection of fatigue damage in the literature, there has been no generalized approach for detection and sizing of crack initiation. Moreover, application of AE-based techniques for in-situ monitoring of small crack growth and initiation has not been adequately developed. Additionally, AE-based probabilistic prediction method for small crack initiation and growth is absent in the literature. Besides being useful, these probabilistic studies can provide researchers with a great deal of insight to the subject.

3 Chapter Three: Large crack growth model validation

3.1 Overview

This chapter focuses on the validation of the AE model for large crack growth assessment. In this chapter, the relationship between crack growth rate and AE signal features generated during crack growth will be validated. Also, the experimental setup and procedures used for fatigue testing will be explained in detail. Additionally, the procedure of probabilistic model development and validation will be discussed and the uncertainties of the model will be investigated. In the model development phase, the distributions of model parameters will be estimated based on a "modeling" set of data. The developed model will be validated later using a new set of data that was not used in model development process. As a result, the model error will be estimated. Model development and validation will be discussed in detail in this chapter. The developed AE model can be used in real time monitoring of structural health.

3.2 Experimental set up

The experimental setup and procedure used as a part of this research to generate the experimental data for model development and validation is described in this section. The AE fatigue experimental data required for developing the statistical model will be discussed later in this chapter.

3.2.1 MTS Testing Machine

Fatigue tests were carried out using a uni-axial load frame Material Testing System (MTS). The MTS used in this study was a model 810, 22 kN load frame with a PC-Per-Station series controller allowing for having a separate computer and monitor for each station and simplified window management and station operation. The testing machine is shown in Figure 3-1.

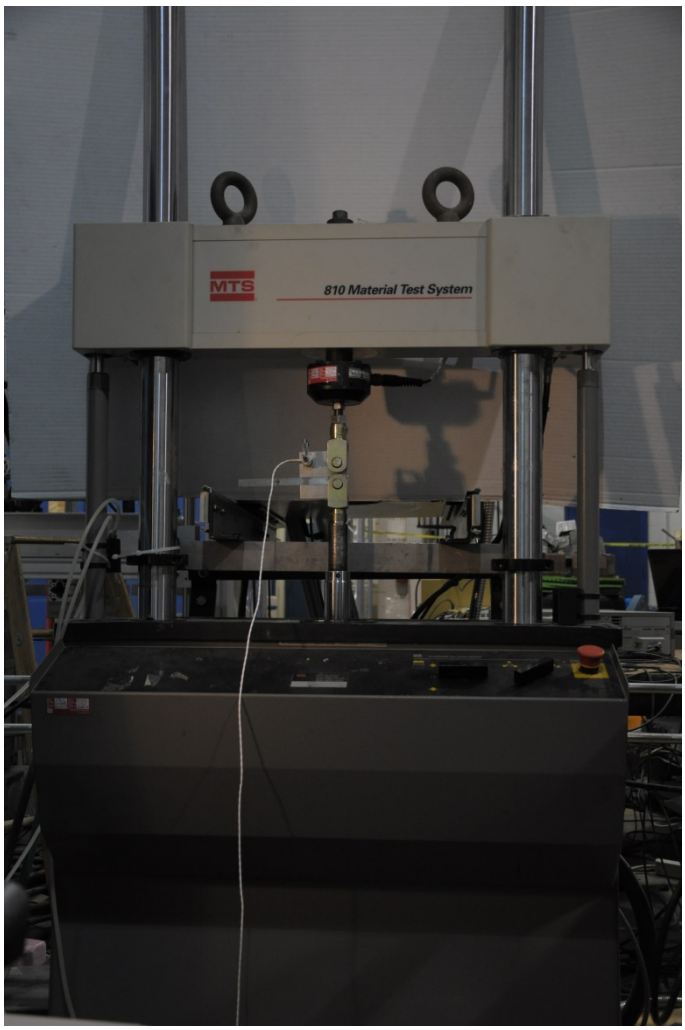

Figure 3-1 MTS Load Frame

3.2.2 Acoustic Emission Instrumentation

An advanced DiSP-4 AE system, supplied by Physical Acoustic Corporation[1], was used to record the AE signals resulting from the propagation of the crack inside the material. This monitoring system consists of four main parts: a single AE Sensor to collect the signals, an amplifier to amplify the resulting signals, a data acquisition module to perform primary filtration and record the signals, and a software module (AEWin) to display the data and perform feature extraction. AEWin is the software used for data acquisition, real time simultaneous AE feature, waveform processing, displaying and fast storage. The DiSP-4 hardware system is controlled via AEWin software.

For all experiments, silicon grease was used as the coupling agent to attach the sensor to the specimen surface in order to take advantage of the extreme sensitivity of the sensor. It enhances the ability of capturing proper signals.

In order to avoid introducing additional uncertainties to the AE signal, an attempt was made to keep the position of the sensor unchanged on the test specimen for all the experiments. A U-shaped clamp was used to hold the sensor firmly on the specimen surface during the tests (see Figure 3-2). A 40 dB preamplifier was used to amplify the AE signals received from the sensor. A band pass filter was used in this amplifier, and amplified signals were analyzed using the DiSP-4 system. The AE data measured and recorded included counts, amplitude and time of the event.

---

[1] www.pacndt.com

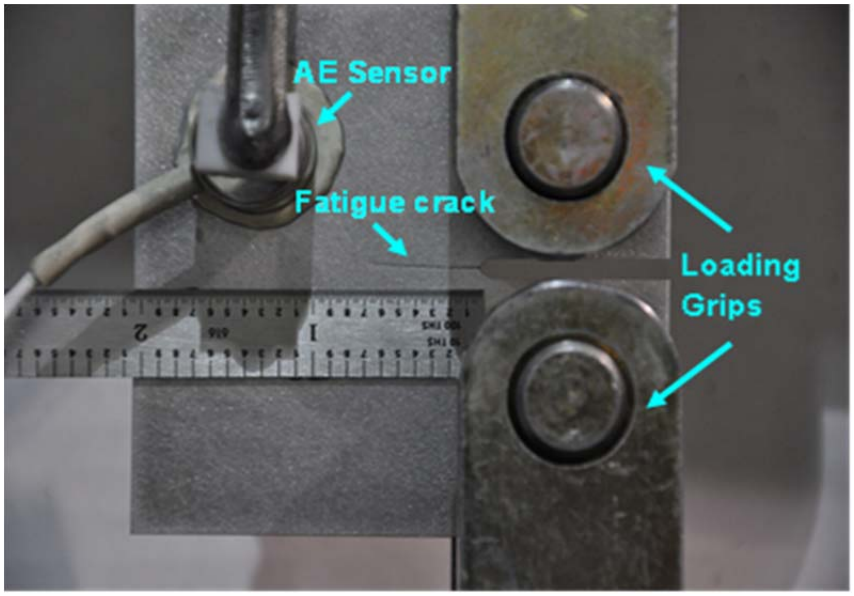

Figure 3-2 Standard CT specimen with mounted AE sensor

3.2.3 Specimens

The goal of the experiments performed was to monitor fatigue crack propagation in standardized specimen. The material used in study of large cracks was aluminum alloy 7075-T6 supplied in the form of compact tension (CT) specimens, based on ASTM standard E647 (2008).This alloy is typically used in aerospace applications.

The test specimens were manufactured from 3.175 mm (0.125 in.) thick plates. The geometry and dimensions of the specimens are shown in Figure 3-3

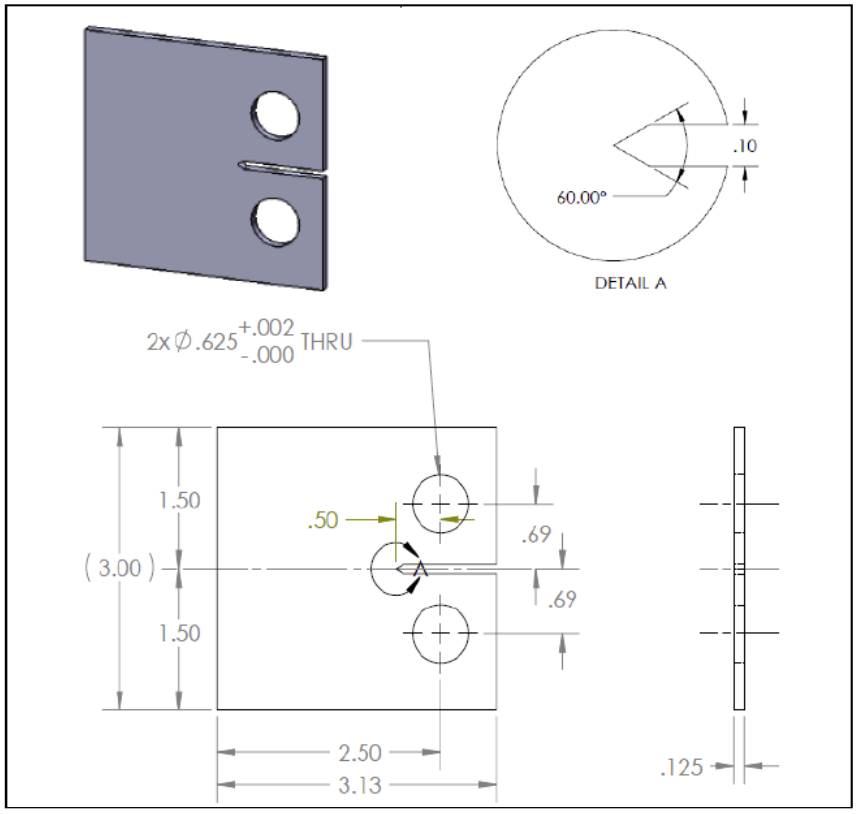

Figure 3-3 .Technical drawing of the CT specimen

3.2.4 Optical detection of cracks and sizing

A time-lapsed photography technique was used to measure crack length during the experiments. A Nikon D-90 digital single lens reflex camera took time-lapsed pictures of the crack growth. A close up lens was used with the camera to capture high-resolution pictures of the specimen. The complete set up is shown in Figure 3-4. As shown in this figure, a scribed ruler was attached to the specimen and was used to

scale the crack length measurement. The delay between taking images was set manually. As a result, a considerable volume of data was captured and stored for further processing. Also, a Java-based image processing program called ImgeJ[2] (Ferreria & Rasband, 2012) was used to post-process the images in order to extract the length of the crack in each image.

Figure 3-4 Test setup for crack measurement using digital photography

[2] ImageJ user guide can be downloaded from: http://imagej.nih.gov/ij/docs/guide

3.3 Fatigue Testing

The CT specimens were instrumented with an AE sensor and mounted on the MTS machine. During the fatigue loading, each test was monitored using AE and time-lapse photography. The load, AE signal and observed crack lengths were recorded and correlated by synchronizing them through the recorded elapsed time. Figure 3-4 shows the experimental set up. For the first phase of this research, in order to study the steady state crack growth (large cracks) constant amplitude sinusoidal loading cycles were applied until a fatigue pre-crack of adequate length and straightness, according to ASTM standard E647 (2008), could be detected. Then, the standard crack growth tests (according to ASTM E647-08) were conducted using the same MTS machine. All the experiments were continued until fracture. Experiments performed on several CT specimens were subjected to cyclic loading of different loading features, such as loading frequency and loading ratio. For each case, one of the loading features was changed with all other test parameters remaining constant. Table 3-1 lists the experiments performed for the corresponding loading ratios and loading frequencies. All the experiments were performed in ambient laboratory air (temperature 20-25°C) with a relative humidity in the range of 50-60 percent.

Table 3-1. Details of experiments and load parameters.

Test Reference	*Loading Frequency(Hz)*	*Loading Ratio (R)*	*Force (min-max) lbf*
CT1	**10**	**0.1**	**50-500**
CT2	**10**	**0.1**	**50-500**
CT3	**10**	**0.3**	**150-500**
CT4	**10**	**0.3**	**150-500**
CT5	**10**	**0.5**	**250-500**
CT6	**10**	**0.5**	**250-500**
CT7	**2**	**0.1**	**50-500**
CT8	**2**	**0.1**	**50-500**
CT9	**7**	**0.1**	**50-500**
CT10	**7**	**0.1**	**50-500**
CT11	**10**	**0.1**	**50-500**
CT12	**10**	**0.1**	**50-500**

The AE transducer described in the previous sections was used to capture AE signals during the standard crack growth tests. The AE threshold of 45 dB was used to capture crack related signals. Meaning, signals with amplitudes exceeding 45 dB were used for this analysis. A 40 dB amplifier was used to amplify the captured AE

signals and then a band-pass filter was used to filter out the part of the noise, resulting mostly from the MTS machine.

Table 3-2 shows a list of controllable AE hardware features available on the PCI-2 board along with their selected values. The selections were made based on the standard ranges (Physical Acoustic Corporation, 2007). This list includes the above-mentioned threshold and band-pass filter (see Table 3-2).

Table 3-2. AE software parameters setting

Parameter	*Value*	*Unit*
Preamplifier	**40**	**dB (decibels)**
Threshold	**45**	**dB**
Sampling rate	**5**	**MSPS (Million Sample Per Second)**
Pre-trigger length	**100**	**µs (Micro second)**
Hit length	**614**	**µs**
High pass analogue filter	**200**	**KHz (Kilo Hertz)**
Low-pass analogue filter	**3**	**MHz (Mega Hertz)**

3.4 Data Analysis and Test Results

AE signals may be generated from a number of possible sources including background noise, micro-crack generation, or plastic deformation. In order to reduce uncertainties and determine the AE signals corresponding to crack growth, applying noise reduction techniques on the captured data is required. Noise reduction

approaches are discussed in the following section, followed by crack measurement method and model development.

3.4.1 Noise reduction

Various de-noising techniques have been proposed to filter AE signals due to crack growth (Morton et al., 1973; Roberts & Talebzadeh, 2003a; Wang et al., 1992).

To filter out noise from acoustic emissions associated with fatigue crack propagation, in the first step, the recorded AE data was filtered using the DiSP-4 source location software. The filtration was done using a band pass filter (200 kHz- 3 MHz) to eliminate emissions from extraneous sources. A detection threshold needs to be determined to filter the background noise (see Figure 2-2). The lack of significant AE activity in the initial stages of loading makes it more difficult to distinguish background noise from fracture-related acoustic events. A dummy specimen without crack was tested under the same conditions as the main experiments. Based on this dummy test, the AE detection threshold was set to 45 dB to eliminate the background noises. This threshold was applied using AEWIN software as well.

It has also been observed that AE events occurring during the loading portion of a cycle are related to crack growth (Morton et al., 1973; Rabiei, 2011; Roberts & Talebzadeh, 2003b). Therefore, the AE data taken during the loading portion of each cycle were used for data analysis. In addition, majority of researchers have assumed that only events occurring close to the maximum or peak load are associated directly with crack growth (Gong Z., DuQuesnay D.L., 1998; Morton et al., 1973; Wang et al., 1992). So, the filtered AE events were separated for different percentages of the

applied load range and it was determined that the AE counts occurring within the top 20% of peak load shows the closest correlation with crack propagation rates.

3.4.2 Crack growth measurement

The lengths of the pictured cracks were measured using the image processing software (ImageJ). Crack measurement at the image processing software was calibrated using the scale ruler attached to the specimen. The accuracy of the ruler was 0.01 inch, therefore, the scale error was estimated to be half, or a value of ±0.005 inches. Since the average measured crack length was about 0.5 inches, the measurement error was calculated to be 1%. It should be noted that since the crack lengths were large enough and a high resolution camera was used, the probability of optical detection of cracks was considered to be equal to 1 for all the experiments. Therefore the measurement error assumed to be equal to one percent. It will be used later to quantify the experimental error in this chapter.

When the crack lengths were determined, the fatigue crack growth rates were approximated at different cycles using Equation (3.1):

$$\frac{da}{dN} = lim_{\Delta N \to 0} \frac{\Delta a}{\Delta N} \tag{3.1}$$

For all specimens studied, good correlation has been obtained between AE count rates and crack growth rates, which do not deviate greatly from linearity during stable crack growth.

Figure 3-5 shows an example of the linear relationship between *log(da/dN)* and *log(dc/dN)* observed in an experiment performed in this study (CT3). Similar correlation was observed for the other experiments (see

Figure 3-6 and

Figure 3-7)

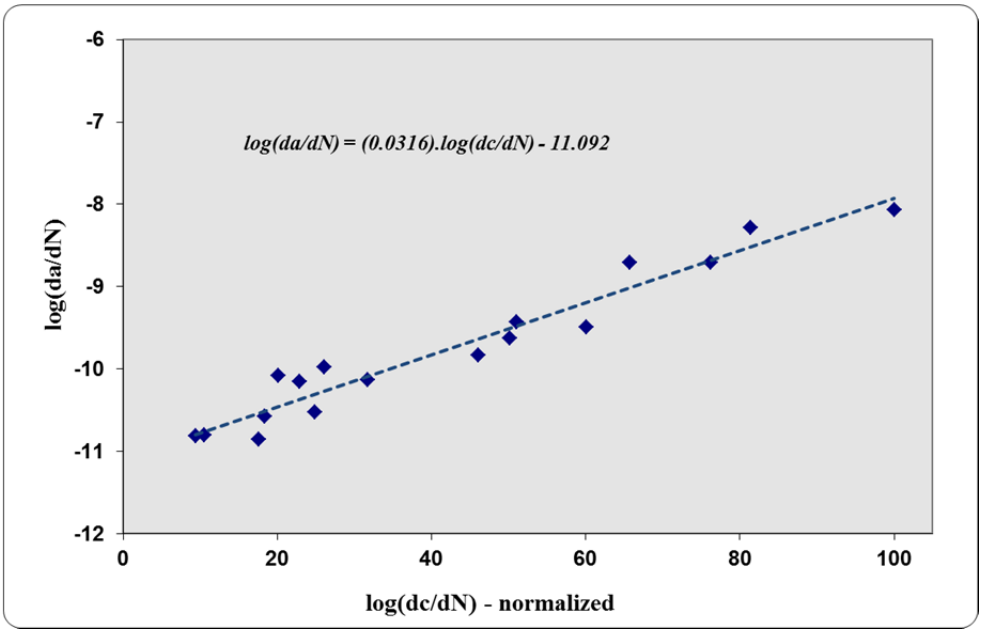

Figure 3-5. Example of a Linear Relation between Crack Growth Rate and AE Count Rate

The correlation between *dc/dN* and *da/dN* of different experiments at different loading ratio are shown in

Figure 3-6.

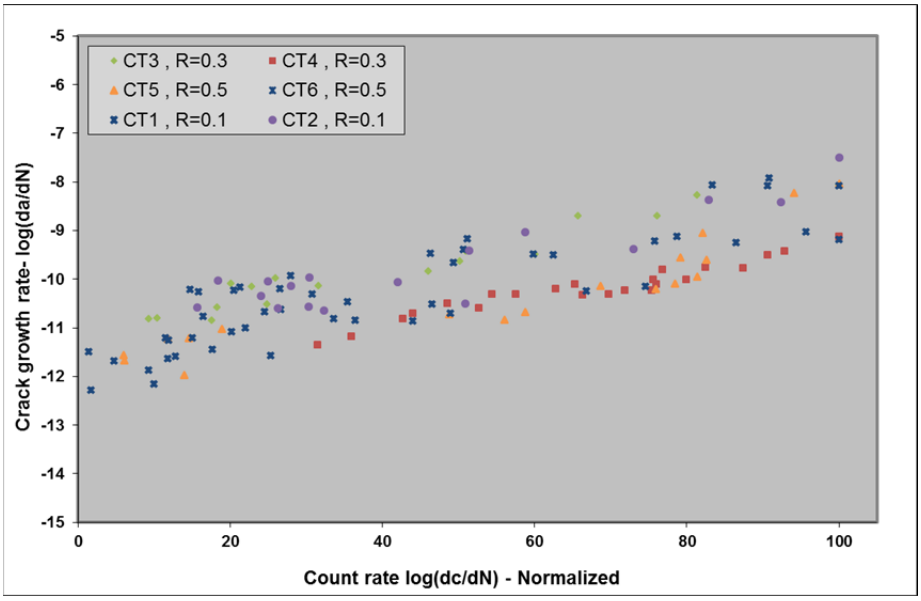

Figure 3-6 Crack growth rate versus AE count rate at different loading ratios

Similar results were achieved for tests at different loading frequencies (see Figure 3-7). The observed correlation of count rates versus crack growth rates and the Bayesian regression analysis of the experimental data corresponding with different frequencies all showed that estimated parameters of the regression line are in the same range and have not any considerable difference. (See the regression results in Table 3-3).

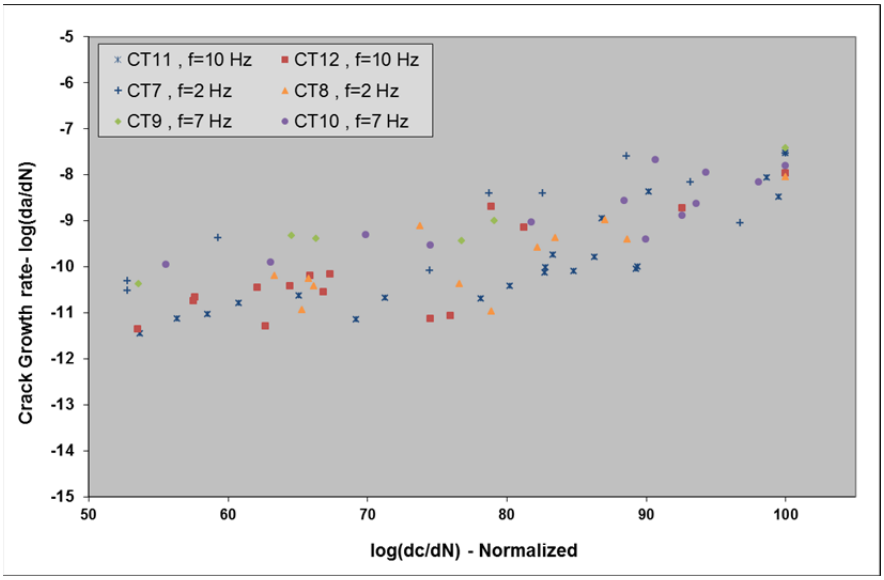

Figure 3-7 Crack growth rate versus AE count rate at different loading frequencies

According to the observed correlation between AE count rates and crack growth rates a log-linear model was used in the form of Equation 2.2.

$$\log\left(\frac{da}{dN}\right) = \alpha_1 \log\left(\frac{dc}{dN}\right) + \alpha_2 + \varepsilon \qquad (2.2)$$

After post processing of AE data, the experimental results were used to estimate the unknown parameters in Equation 2.2 using regression analysis. The parameters of the linear regression model were estimated and compared for the different experiments listed in Table 3-1. A summary of estimated mean parameters for each experiment is presented in Table 3-3 for comparison.

Table 3-3. Regression parameters for individual test data

Test	Freq.	R	α	β
CT1	10	0.1	0.0351	-11.461
CT2	10	0.1	0.0313	-11.179
CT3	10	0.3	0.0316	-11.092
CT4	10	0.3	0.0271	-12.019
CT5	10	0.5	0.0304	-11.971
CT6	10	0.5	0.028	-11.775
CT7	2	0.1	0.0276	-10.883
CT8	2	0.1	0.0512	-13.862
CT9	7	0.1	0.0283	-10.865
CT10	7	0.1	0.0237	-10.742
CT11	10	0.1	0.0465	-12.916
CT12	10	0.1	0.0475	-13.419

Table 3-3 shows that there is no considerable effect of different loading conditions on the estimated model parameters and subsequently on the crack growth behavior.

3.5 Test of Homogeneity

The fractional analysis method of ANCOVA was used to determine if there is any significant statistical difference in the regression lines achieved from different test data. The topic of interest is whether the regression lines are parallel (i.e., the slopes are equal). Since there are more than two regression lines, the procedure of

ANCOVA was used to compare multiple regression lines. This method allows for testing the null hypothesis that the regression model parameters were derived from samples estimating populations which all had equal slopes:

$$H_0: \alpha_1=\alpha_2=\alpha_3 \ldots =\alpha_k \tag{3.2}$$

While the alternative hypothesis is that at least two of the regression model slopes are significantly different. ANCOVA also tests the hypothesis that the intercepts of the regression models are equal which are verified to come from populations with equal slopes. ANCOVA was used to compare the linear relationships between *da/dN* and *dc/dN* at different loading conditions. An *F* statistic was computed as:

$$F = MS_{RC} / MS_p \tag{3.3}$$

The pooled mean square (MS_p) is the average MS residual of all the linear relationships involved in the analysis. The regression coefficient MS (MS_{RC}) expresses the variation resulted from differences between slopes. The smaller MS_{RC}, the closer the slopes would be. MS_{RC} increases as the regression lines diverge from each other. This leads to a one sided test with the null hypothesis (H_0) that the regression coefficient MS will be less than the pooled MS.

$$H_0: MS_{RC} \leq MS_p \tag{3.4}$$

where the alternative hypothesis is defined as:

$$H_1: MS_{RC} > MS_p \tag{3.5}$$

If H_o is not rejected then it can be concluded that the slopes are statistically similar; however, if H_o is rejected then the slopes are considered to be different. MS_p is calculated by averaging MS residual of all regression lines involved and the regression coefficient MS (MS_{RC}) is the difference between the unexplained variation of an "average" slope (common MS) and the unexplained variation averaged from all the lines involved (MS_p). For more information about computation of MS_{RC} and MS_p refer to (G. A. Miller & Chapman, 2001; Smith, 1975)

The results of ANCOVA are listed in Table 3-4. The F statistics is displayed in the ANCOVA results to test H_0 using Eq. (3.4). It should be noted that $P_{critical}$ is equal to 0.05 for 90% confidence limit level. The probability corresponds to the F statistics $(P(F_{[0.05,k,df]}))$ is also calculated and found to be greater than $P_{critical}$. The null hypothesis of H_0: $MS_{RC} \leq MS_p$ was accepted because F statistic is less than unity and P-value is greater than $P_{critical}$ .It means that the null hypothesis should not be rejected. It can be concluded that there is no statistically significant difference between the slopes of regression lines.

Table 3-4. ANCOVA output

ANCOVA Results

(k=12) **Test for Homogeneity of Regressions**					
Source	***SS***	***df***	***MS***	***F***	***P***
Between Regressions	**2.47**	**11**	**0.22**	**0.82**	**0.6185818**
Remainder	**58.31**	**213**	**0.27**		

The ANCOVA results show that, the model is not influenced by the loading ratio and loading frequencies. As such changes in loading conditions did not support any significant influence on crack growth and the resulting AE signals.

Since the results show that changes in certain loading conditions do not result in any significant influence on the linear model of AE count rate vs. crack growth rate, all the experimental data from different tests could be used to develop the model. In order to do this, the experimental data set was divided to three different sets. Two sets were used for modeling (one for parameter estimation and one set for evaluating the error term in the model) and final data set was used for model validation. For discussion on model development see section 3.7. The number of four experiments was pooled together to arrive at a more generic model in the phase of model development. Those experiments were selected from different loading conditions as listed in Table 3-5. Later, the second set of data (six more experiments which were not used in modeling and listed in Table 3-6) were used to estimate the uncertainties and capture the error term in the model. The last step was to validate the developed model. The experiments used for validation are listed in Table 3-7. The procedure and results of model development and validation are reported in the remainder of this chapter.

3.6 Bayesian Data Analysis

In this research, a Bayesian regression approach was implemented for parameter estimation. This technique is used to estimate and update the posterior distribution of

the unknown model parameters. The Bayesian probabilistic modeling is described in this section.

Bayesian analysis is different from classical statistical analysis since all the unknown parameters are considered random variables (Ntzoufras, 2009). Bayesian statistic is developed based on Baye's theorem and can be summarized as (Bolstad, 2007)

$$Posterior \propto Prior \times Likelihood \tag{3.6}$$

The prior includes any information available about the data involved in Bayesian analysis. What is of interest is the posterior distribution of the model parameters (θ) given the observed data (x) as it is shown mathematically in Equation (3.7). In the Bayesian inference a prior pdf of parameters is combined with observed data (evidence) in the form of a likelihood function of an unknown parameter θ. The result is an updated state of knowledge in the form of a posterior pdf, $f(\theta|x)$.

The posterior distribution of model parameter can be assessed as described according to Baye's theorem as:

$$f(\theta|x) = \frac{f(x|\theta)f(\theta)}{f(x)} \propto f(x|\theta)f(\theta) \tag{3.7}$$

Where $f(\theta \mid x)$ is the posterior distribution of the parameters (θ) given the observed data (x). $f(x)$ is the marginal density function of random variable x, $f(\theta)$ is the prior distribution of the model parameters; and $f(x \mid \theta)$ is the likelihood of the model and contains the available information provided by the observed samples:

$$f(x|\theta) = \prod_{i=1}^{n} f(x_i|\theta) \tag{3.8}$$

The Bayesian framework is shown in Figure 3-8 (Azarkhail & Modarres, 2007).

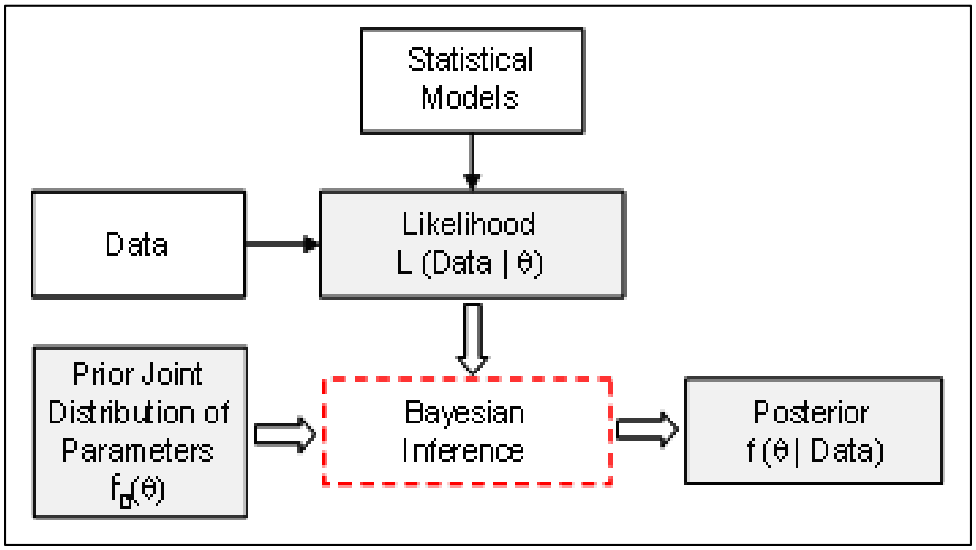

Figure 3-8. Bayesian Inference Framework (Azarkhail & Modarres, 2007)

3.7 Probabilistic Model Development

The results of the analyzed experimental data were used to develop a probabilistic linear model for the estimation of the crack growth rate as the dependent variable, and using the AE count rate as the independent variable. As discussed in Chapter 2, the AE-based model proposed previously by Rabiei (Rabiei, 2011) showed that on average a log-linear relationship can be assumed between crack growth rate (*da/dN*) and AE parameter (*dc/dN*) (See Equation 2.2.) This model was proposed based on a single experiment and was not validated with more experimental data. In this research

the adequacy of the proposed model was reviewed based on the additional experimental data obtained in the last sections (see Table 3-1 for details). Post processing of data showed similar correlation existed at different loading conditions (as described in the previous sections). So, based on the observed correlation the unknown parameters of the linear model described in section 2.3.1 are updated. An error term was added later to assess the model error. Eventually, the structure of the probabilistic model will be similar to the proposed model from Rabiei's work (Rabiei, 2011):

$$\log\left(\frac{da}{dN}\right) = \alpha \log\left(\frac{dc}{dN}\right) + \beta + \varepsilon \tag{3.9}$$

This error term (ε) is the model error that accounts for difference between the model prediction and the observed AE count rate and follows a normal distribution with the mean of zero and standard deviation of σ.

$$\varepsilon \approx N(0, \sigma) \tag{3.10}$$

In the remainder of this chapter, Bayesian regression analysis will be used first to compare fitted model parameters for different experimental condition and observe any possible effect of loading conditions on the results. Then the experimental data obtained in the previous section will be divided into three different sets, one set will be used for modeling and the second set will be used for estimation of probabilistic error in the model, and the last set will be used for model validation. The probabilistic model development is discussed in detail in the remainder of this section.

After first steps of analyzing the experimental data including crack growth measurement, AE data filtration and calculating count rates, the results were used to estimate the marginal and joint distribution of the unknown parameters in Eq. (3.9) using the Bayesian regression analysis. The software package WinBUGS (Ntzoufras, 2009) was used to perform the Bayesian inference. In this Bayesian inference the likelihood function of the observed independent crack data points (x_i, y_i) can be expressed as a normal distribution:

$$p\left(D\middle|\alpha_1,\alpha_2,\gamma_1,\gamma_2\right)=\prod_{i=1}^{n}\frac{1}{\sqrt{2\pi\sigma}}\exp\left(-\frac{1}{2}\left(\frac{y_i-\left(\alpha_1 x_i+\alpha_2\right)}{\gamma_1\exp\left(\gamma_2 x_i\right)}\right)^2\right) \tag{3.11}$$

where $x_i=log(dc/dN)_i$, $y_i=log(da/dN)_i$ and D is the data set of pairs (x_i, y_i) for $i=1$ to n.

Table 3-5.Experiments selected for model development

Test Reference	Loading Frequency (Hz)	Loading Ratio (R)	Force (min-max) lbf
CT1	10	0.1	50-500
CT3	10	0.3	150-500
CT5	10	0.5	250-500
CT7	2	0.1	50-500

Table 3-6. Experiments used for error estimation

Test Reference	Loading Frequency (Hz)	Loading Ratio (R)	Force (min-max) lbf
CT2	10	0.1	50-500
CT4	10	0.3	150-500
CT6	10	0.5	250-500
CT8	2	0.1	50-500
CT10	7	0.1	50-500
CT12	10	0.1	50-500

Table 3-7. Experiments used for model validation

Test Reference	Loading Frequency (Hz)	Loading Ratio (R)	Force (min-max) lbf
CT9	7	0.1	50-500
CT11	10	0.1	50-500

3.7.1 Regression analysis

The model parameters were determined using least square regression analysis. Table 3-8 listed the regression mean results using data from modeling experiments (listed in Table 3-5). Figure 3-9 shows the estimated linear model parameters considering all data from modeling experiments listed in Table 3-5.

Table 3-8. Estimation of the model parameters

Model Parameter	*Regression Estimation*
α	**0.0303**
β	**-11.319**

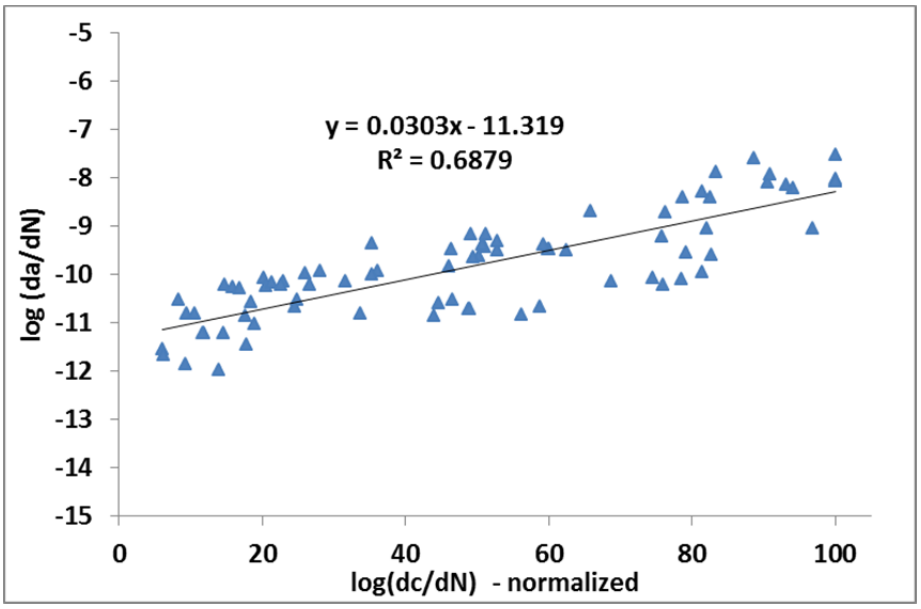

Figure 3-9. Linear regression result

3.7.2 Error and Uncertainty

Uncertainties associated with the model have various sources which may be grouped as follows:

a) Aleatory uncertainty: Also, known as inherent uncertainty, is a natural randomness of a quantity such as uncertainty in the material features. Generally, there are different factors during manufacturing of a material that cause random variation of the material property from experiment to experiment (Ditlevsen & Madsen, 2007). In order to reduce this aleatory uncertainty, an attempt was made to use test data of specimens from the same batch of aluminum (test samples coming from the same sheet of Al7075-T6). It should be noted that this physical variation are inherent to experiments and cannot be completely eliminated.

b) Epistemic uncertainty: This uncertainty is the result of limited information or incomplete information due to finite experimental data or limited number of observed data points. Addition of experiments corresponding with each loading condition in the parameter estimation process can help reducing epistemic uncertainty bounds for the estimated model parameters. Two types of epistemic uncertainty are discussed below:

1. Measurement error: This is error caused by imperfect measuring equipment and/or human observation errors. There are some inherent variations resulting from the method of observation. Usually, two different measurement equipment used on the same material can result in significant difference between measurements. On the other hand, the image processing method used for measuring the specimen's crack length based on the high resolution photography with the close-up lens carries some measurement errors due to difficulties in finding the crack tip in images.

Some methods applied to reduce the crack length measurement error. If the measurement value is known to be constant from one measurement to another and also if the measuring method can be applied several times to the object, by a series of repeated measurements, information about the uncertainty of the measuring method can be obtained and this uncertainty can be reduced through averaging. In this research, an attempt was made to reduce the measurement uncertainty using the measurement data produced by two different individual testers on each data point. Since these measurements are mutually independent the mean value of the measured crack length was used at each point.

2. Modeling error: Beside the error because of crack length measurement,

material variability, filtration method and insufficient data, there is an important model uncertainty that must be captured. This is model uncertainty which relates to the formulation of the proposed probabilistic model and is due to imperfections in physical model formulation as well as in choice of probability distribution types for representation of uncertainties.

There might be some other sources of uncertainty that can be considered such as the uncertainty resulting from the de-noising technique. The noise reduction method may filter out some crack growth related signals as well. Improvement can be made by exploring alternate methods of classification of AE-related data and filtration techniques. In the next section the AE model error is estimated which expresses the sum of aleatory and epistemic uncertainties described above. Later in section 3.8 the model is validated and the uncertainties are estimated.

3.7.3 Model Error Estimation

After establishing a linear relationship between the explanatory variable *dc/dN* and the response variable *da/dN* (Eq. (3.9)), this relationship shall be used to make predictions of the next value of crack growth rate given the next value of count rate. Making prediction of future observations for specified *dc/dN* values is one of the main goals of linear regression modeling. Better prediction can be made considering the uncertainties and errors in the model. The best prediction for $(da/dN)_{n+1}$ given $(dc/dN)_{n+1}$ will be:

$$\log\left(\frac{da}{dN}\right)_{n+1} = \hat{\alpha}\log\left(\frac{dc}{dN}\right)_{n+1} + \hat{\beta} + \varepsilon \qquad (3.12)$$

Where $\hat{\beta}$ is the slope estimate and $\hat{\alpha}$ is the estimate of the intercept (see Eq. (3.9)). The error term showed by ε includes all the uncertainties discussed in last section and follows a normal distribution with the mean of zero and standard deviation that needs to be captured. True values for model parameters are unknown and using estimated values in the prediction adds an uncertainty that should be captured by the error term.

The error estimation was performed by comparing experimental measurements (using tests listed in Table 3-6) with estimated model predictions obtained through Bayesian analysis (using parameter estimation in Table 3-8). The software Winbugs was used to capture the distribution of error term in the model. The posterior distributions of the error term and the corresponding standard deviation were determined subsequently as $\sigma \sim N(0.86, 0.057)$ and $\varepsilon \sim N(0, \sigma)$. The results are shown in Figure 3-10.

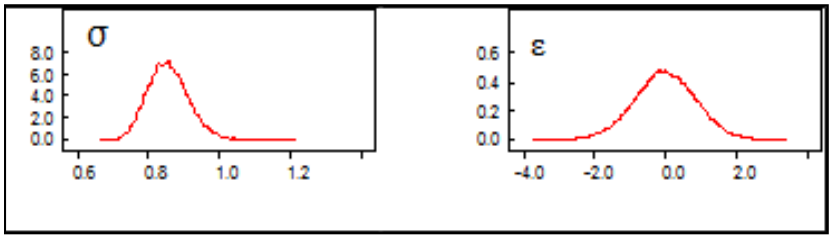

Figure 3-10. Estimated error term

Uncertainties of the model were described via probability distribution functions and the posterior distributions of the model output can be determined subsequently. Using

the developed model, for a given value of *dc/dN*, a distribution of crack growth rate (*da/dN*) can be estimated. The outcome of the proposed model can be used as evidence in a Bayesian updating process to obtain estimation of crack growth rate at different number of loading cycles and improve prognosis results. The result of the posterior predictive distribution for *da/dN* as a function of *dc/dN* is plotted in Figure 3-11. The posterior distribution is shown by its median and the 95% confidence level (2.5% and 97.5% prediction bounds). The data used to fit the model is also plotted in this figure. Figure 3-11 illustrates the posterior predictive Bayesian regression results using data from experiments listed in Table 3-6. The confidence bounds of the posterior predictive model estimation are also shown in Figure 3-11 with 95% confidence level.

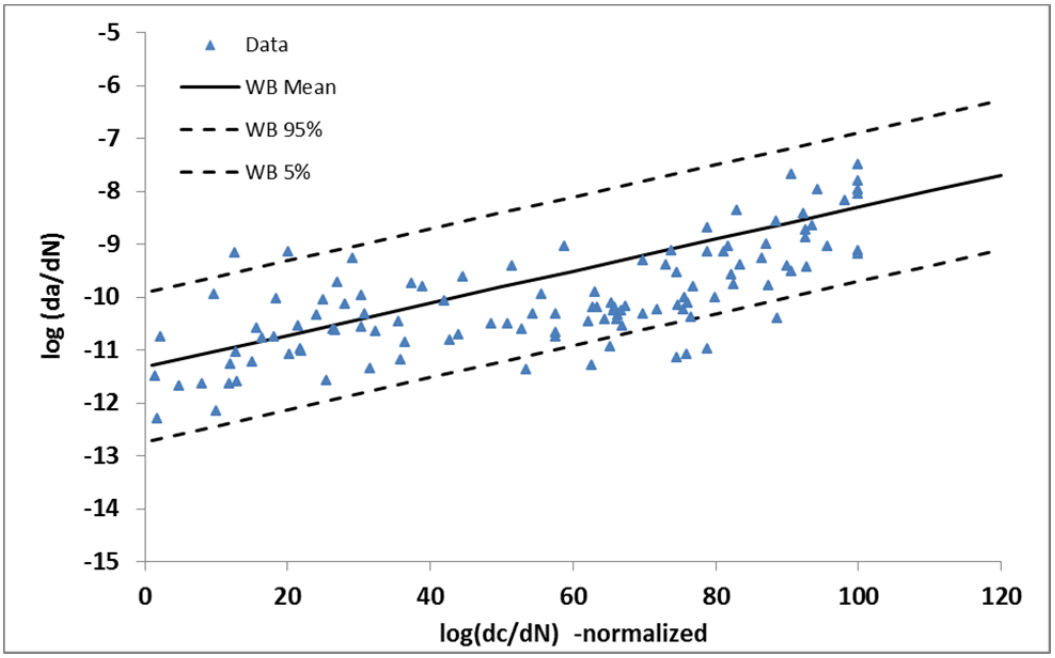

Figure 3-11. Posterior predictive model with the uncertainty bounds

3.8 Model Validation

Model validation is an iterative process that can be defined as the process of determining the model accuracy in representing its intended application in real word. The main activity in model validation is comparison of the estimated model predictions to the experimental results that were not used for model development. The differences between the prediction results computed using the fitted model and the observed experimental results is the model error originated from different sources of uncertainty.

First, a qualitative validation of the developed model was performed using graphical comparisons between model predictions and experimental data and then a more advanced model validation methodology was implemented and the uncertainties of the model prediction were estimated.

Using Bayesian regression for a given value of *log(dc/dN)*, a distribution of *log(da/dN)* was estimated based on the developed AE-based model. The prediction results are then compared against the experimentally observed crack growth rate for two validation tests (CT9 and CT11). Results are shown and discussed below.

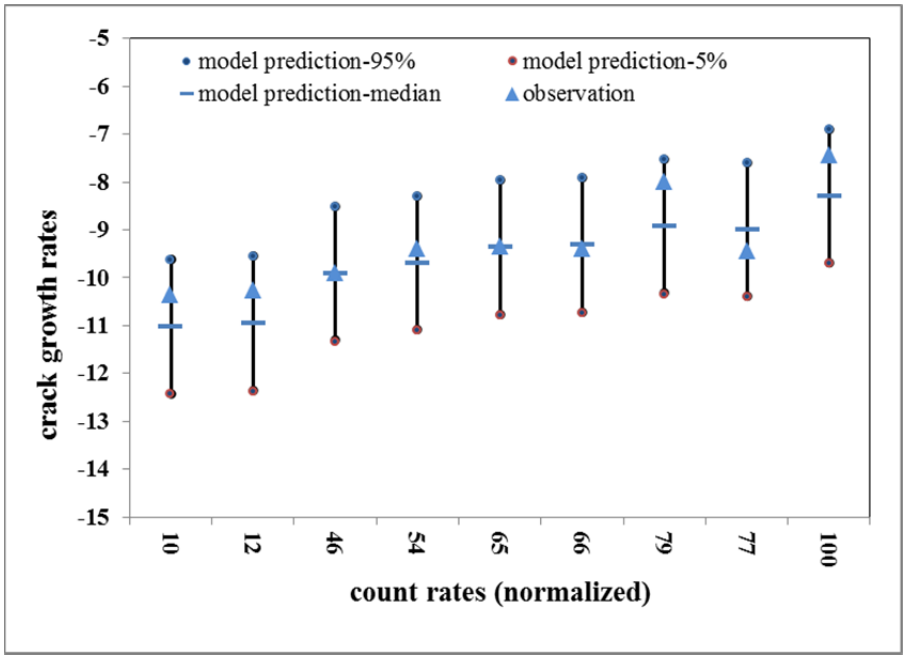

Figure 3-12. Graphical comparison of model prediction and experimental observation (CT9)

Figure 3-12 shows a graphical comparison between the median AE model prediction and experimental observation of crack growth under different count rate values for CT9 (see Table 3-7). The top/bottom points in

Figure 3-12 are correspondingly the estimated 95% and 5% value of model predictions of crack growth based on data observed in AE experiments. The dashed markers are the median values of predictions and the triangle markers show the average values of the observed data. A more detailed graphical comparison between model-predicted measures of response and the experimentally obtained measures of response for experiment (CT9) is shown in Figure 3-13 with the 90% confidence bounds. Figure 3-13 and Figure 3-15 show the model prediction resulting from the Bayesian analysis using 30000 iterations of simulation for each single measurement

of experiments CT9 and CT11. They also show the 90% confidence interval (shown as dashed lines) on the total model predictions. These bounds are estimated using Gibbs sampling from the population of the Markov Chain Monte Carlo predictions (used in Bayesian regression analysis) such as 5% of the predictions are equal or above the upper bound and 5% are equal or below the lower bounds.

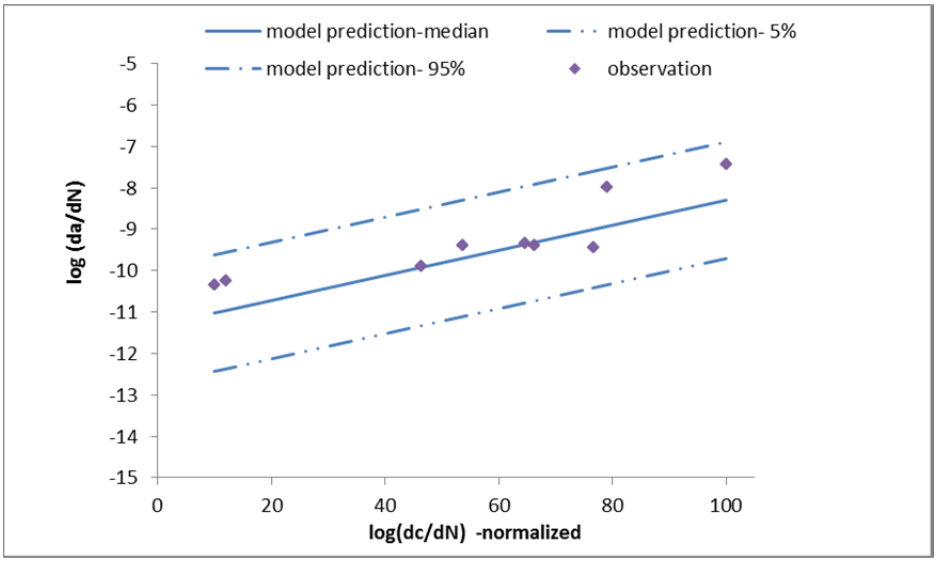

Figure 3-13. Model prediction versus experimental results (CT9)

Result shows crack growth rate estimated for experiment CT9 and the actual crack growth observed are superposed and are in a good agreement. Identical Bayesian analysis procedure was applied on experimental data from test CT11 and the results show similar agreement with the model prediction. Graphical comparisons between model-prediction and the experimentally obtained measures of crack growth rates for experiment (CT11) are shown with the 90% confidence bounds in Figure 3-14 and Figure 3-15.

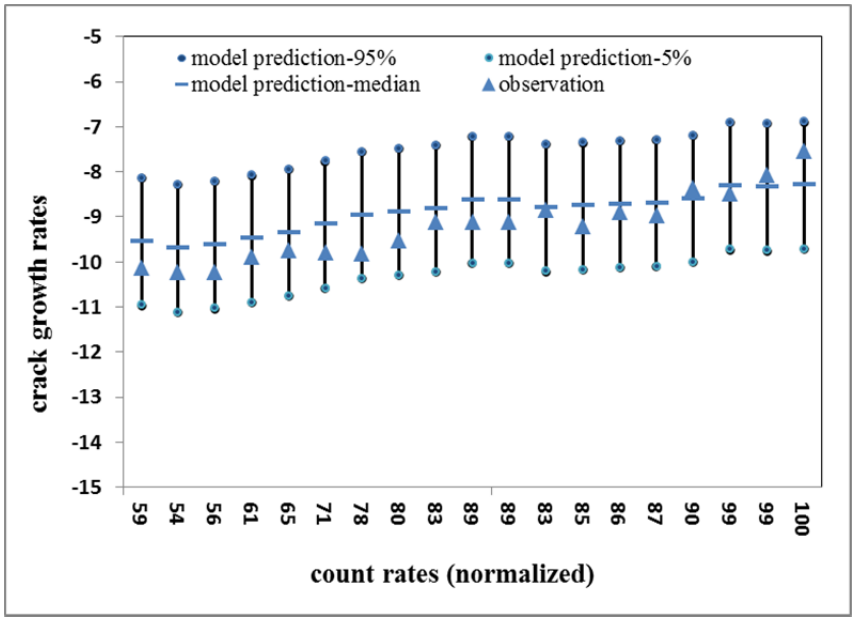

Figure 3-14. Graphical comparison of model prediction and experimental observation (CT11)

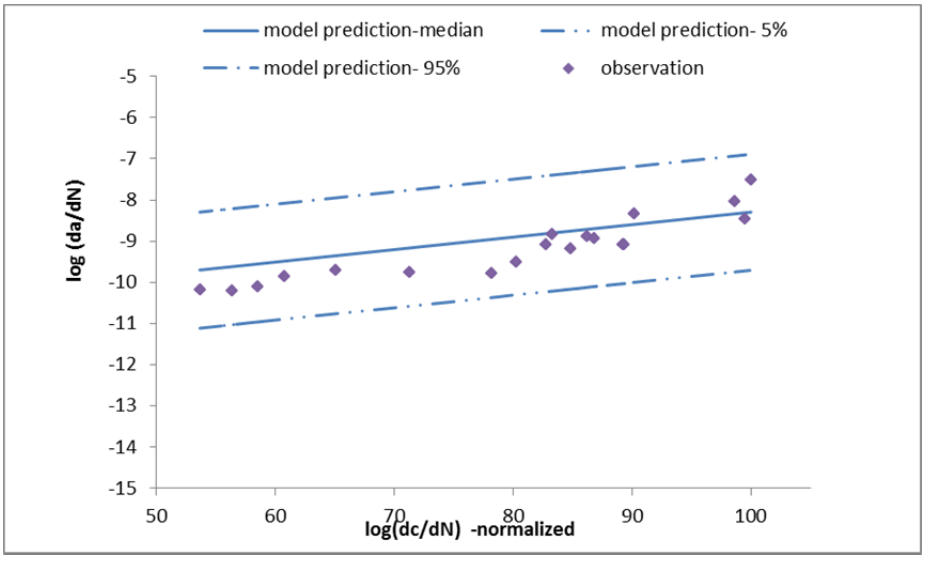

Figure 3-15. Model prediction versus experimental observation (CT11)

The Graphical representation of model validation showed that the experimental measurements of *da/dN* at each *dc/dN* are well within the 90% confidence bound. This indicates that the model is consistent with the experimental results, given the uncertainty in the model prediction.

An additional step toward model validation was performed using a more advanced simulation-based methodology that was employed to validate the model based on a Bayesian estimation approach. This method was developed thru earlier research at the University of Maryland (Ontiveros, Cartillier, & Modarres, 2010) to account for uncertainties within the results of a fire model simulation predictions. In this research the proposed probabilistic approach (Ontiveros et al., 2010) is implemented using the validation sets of data (Table 3-7) to evaluate the errors associated with the developed AE-model and review its prediction uncertainties.

To validate the model prediction, data from experiments CT9 and CT11 (Table 3-7) were used for comparison with the model output. As was mentioned before, these experiments were not used in the development and updating of the model parameters. Available information captured from experimental data was used as the input to the Bayesian estimation procedure. The Bayesian estimation approach updated the model prediction with the experimental results. With this Bayesian estimation inference, uncertainties in the experimental values are propagated in the model and resulted in model prediction uncertainty assessment.

In the proposed model validation methodology (Ontiveros et al., 2010), both model prediction and experimental results are considered to be estimations and representation of the true values, given some error as it is shown in Eqs. (3.13) and (3.14):

$$\frac{X_i}{X_{e,i}} = F_{e,i}\ ;\ F_e \sim LN(b_e, s_e) \qquad (3.13)$$

and

$$\frac{X_i}{X_{m,i}} = F_{m,i}\ ;\ F_m \sim LN(b_m, s_m) \tag{3.14}$$

In which X_i is the true value, $X_{e,i}$ and $X_{m,i}$ indicate the experimental results and model prediction respectively. F_e is the multiplicative error of experiment with respect to true value and F_m is the multiplicative error of the model prediction, with respect to true value. A multiplicative error of experiment with respect to the model prediction is defined by Eq. (3.15):

$$\frac{X_{e,i}}{X_{m,i}} = \frac{F_{m,i}}{F_{e,i}} = F_{t,i} \tag{3.15}$$

$F_{t,}$ is a distribution of the ratio of the experiment and model predictions resulting from multiple iteration of modeling for each experimental data point and can be expressed in the following form:

$$F_t \sim \int_{b_m, s_m} LN\left(b_m - b_e, \sqrt{s_m^2 + s_e^2}\right) \cdot g(b_m, s_m) db_m ds_m \tag{3.16}$$

Where $g(b_m, s_m)$ is the joint pdf of parameters b_m and s_m.

In this approach the likelihood was used as is shown in Eq. (3.17):

$$L\left(X_{e,i}/X_{m,i}, b_e, s_e \middle| b_m, s_m\right)$$

$$= \prod_{i=1}^{n} \frac{1}{\sqrt{2\pi}\left(\frac{X_{e,i}}{X_{m,i}}\right)\sqrt{s_m^2 + s_e^2}} exp\left(-\frac{1}{2} \times \frac{\left[ln\left(\frac{X_{e,i}}{X_{m,i}}\right) - (b_m - b_e)\right]^2}{s_m^2 + s_e^2}\right) \tag{3.17}$$

For more information about the validation method refer to the work of V. Ontiveros (Ontiveros et al., 2010).

Using the validation sets of data the validation approach was implemented and the results are discussed in this section. For simplicity the distribution of model predictions will be reduced to a mean value and compared one-to-one with the experimental results. The mean and standard deviation of F_e, which are b_e and s_e were determined from the unbiased experimental error of ±1% as was discussed in section 3.4.2. The values determined were -0.00002 for b_e and 0.002 for s_e. The summary statistics for the marginal posterior pdf of parameters b_m and s_m as well as the distribution of F_m are presented in Table 3-9.

Table 3-9. Model validation statistic summary

Parameter	*Mean*	*Standard Deviation*	*2.50%*	*median*	*97.50%*
b_m	0.009225	0.01145	-0.01336	0.009239	0.03169
s_m	0.05933	0.008683	0.04522	0.05838	0.07891
F_m	1.011	0.06196	0.8946	1.009	1.141

The model uncertainty bounds for the crack length estimation can be determined from the 2.5 and 97.5 percentile of the multiplicative error of F_m. The resulting upper bound on reality was calculated as 14%, while the lower bound is -10%. These results are presented graphically in Figure 3-16.

It can be noticed that the mean values of the model prediction are standing on the upper bounds of the experimental error and the value of F_m for the model prediction is

greater than 1. The value of F_m around 1.01 suggests a very small bias in the AE model to under predict the true crack growth rate. Therefore, the estimation of true crack growth rate given the model prediction is expected to be slightly higher. The results show that to correct the model, the predictions must be increased by a factor of 1.01.

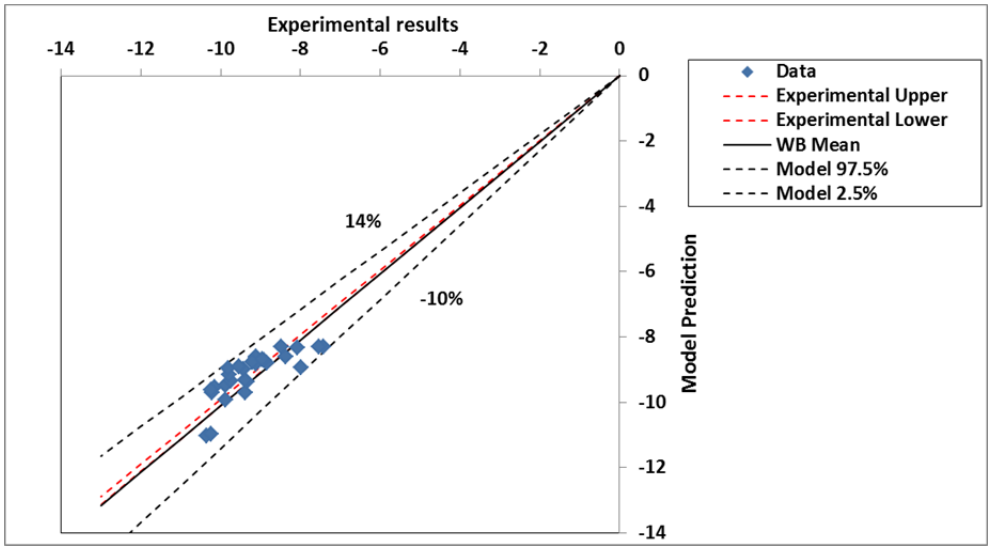

Figure 3-16. Comparison of AE model prediction and experimental results

As expected, the validation results showed good agreement between model predictions and experimental observations. The validated AE model can be used in real time monitoring of large cracks that subsequently improves the structural health management. The application of AE monitoring methodology for detection of small cracks will be discussed in the next chapter.

4 Chapter Four: Small crack growth and crack initiation

4.1 Overview

One of the challenging problems in of the field of fracture mechanics is the detection of crack initiation as well as prediction of small crack growth in early stages of propagation. Although behavior of small cracks is an extremely complex subject, due to the importance of small crack detection in SHM, it cannot be ignored. Many researchers have worked on small cracks and there are various published data as the result of experiments on small crack in the literature. Moreover, several models to simulate the small crack growth behavior exist in the literature (some examples include Forth et al., 2005; Künkler et al., 2008; McDowell, 1997; Shyam et al., 2005), but no conclusive AE-based experimental study on detection of crack initiation has been reported and consequently no AE-based model for small fatigue crack growth is available.

In the current chapter a novel methodology of statistical AE data analysis for detecting crack initiation and developing a probabilistic AE model of small crack growth is introduced. Also, a relationship between small crack length and AE signal features generated during crack growth is developed. The experimental setup and procedure used in fatigue testing is also explained in detail. Moreover, the procedure of probabilistic model development and validation is discussed and the uncertainties of the model are reported.

4.2 Fatigue Crack Initiation and Small crack

There is no universally accepted definition for fatigue-induced "small crack" and "crack initiation". Most experts consider cracks less than *1mm* in length ($a < 0.001$ *m*) as small (Anderson, 1995; Larsen & Allison, 1992). Fatigue crack initiation is a subjective notion as well. Some consider crack initiation as corresponding with a fatigue phenomenon and some associate it with an arbitrarily specified crack length. For example, the U.S. Navy defines the presence of a crack 250 μm in length, as the point where crack initiation occurs (Iyyer et al., 2007; Papazian et al., 2009). Furthermore, others consider a crack length ranging from a size of grain diameter to about 100 μm as crack initiation length depending on material and scale of interest. However, ranges of values have been used for identification of crack initiation in different materials within the literature [e.g., 51 μm for carbon steel, 120 μm for BS250A53 steel and 1 mm for En7A steel (Bhattacharya & Ellingwood, 1998) and up to 500 μm for aluminum (Pearson, 1975)].

A multi-stage fatigue approach developed at the Mississippi State University (Xue, McDowell, Horstemeyer, Dale, & Jordan, 2007) divided the fatigue life of structure into three different stages of incubation, physically small crack growth and large crack growth. In their approach the incubation itself was assumed to be broken to two sub-stages of cracking of a constituent particle and the initiation of a crack in the adjacent matrix material. Based on this work, a SHM study by M. Papazian and his co-workers at Northrop Grumman described the definition of physically small crack

lengths to be between the incubated size (starting from 2 μm) and a crack length that is treatable by linear elastic fracture mechanics, which is about 250 μm for Al7056-T651 (Papazian et al., 2009).

In the current research, a subjective fatigue crack initiation length was used for Al7075-T6. This selection was primarily made based on the limitations in the crack size measurement method (i.e., optical microscopy) used in this study rather than a specific fatigue phenomenon. As such this study uses a subjective crack length of 50 μm as the point of crack initiation. The reasons and limitations of this selection are discussed in sections 4.3.2, 4.5.2 and 4.5.4. It is determined, however, that this crack initiation length is about a quarter of the average grain diameter for Al7075. It has been shown that approximately a $1mm^3$ of the above-mentioned material contains 700 grains (Papazian et al., 2009). Assuming spherical geometry of grains, the volume of each grain is about 1.43×10^{-3} mm^3 and the diameter of each grain can be estimated as 0.140 mm (140 μm). Moreover, the applied optical crack measurement method carries some limitations for sizing of smaller cracks. More detail on the methodology and its limitation are discussed in sections 4.3.2, 4.5.2 and 4.5.4.

4.3 Experimental set up

To study the relationship between small crack length and the resulting AE signal, a group of standard experiments was performed under a controlled loading condition. In this section experimental procedures including specimen selection, test set up, fatigue testing, crack length measurement and AE data acquisition are presented.

4.3.1 Specimen

It is very difficult to capture the microscopic crack growths at the first stage of crack propagation. Among various test techniques that have been used to record the growth of small fatigue cracks, only a few can provide useful measurements of small-crack growth (Forth et al., 2005; Larsen & Allison, 1992). Some measurement methods involve stopping the test to observe and measure the length of small crack. Obviously, these methods provide post-test information, making real-time monitoring of the small crack behaviour impossible. It is desirable to not only measure crack length and crack growth rate of small fatigue cracks, but to do so in real time in order to correlate the state of damage to AE signal properties.

Since in this research the observation of small crack length was done through optical microscopy, a new set of test specimens with the capability of being used for small crack monitoring were developed based on the ASTM standard ("ASTM E466 : Standard practice for coducting force controlled constant amplitude axial fatigue tests of metallic materials," 2012). Series of standard flat dog-bone samples were used in this study which are more applicable for crack initiation tests while in study of large cracks, CT samples were used with a V-shape notch. Since presence of this type of notch causes stress concentration at the notch tip, it is not recommended for study of crack initiation. A U-shape notch made in the dog-bone samples helped to reduce the stress concentration and made it more applicable for crack initiation tests. Also, with the smaller radius of the notch, a higher optical zoom was achieved and resulted in

more accurate measurement of crack length. In addition to that, the structure of the flat dog-bone samples provided the opportunity of direct attachment of the sample to the MTS grips. One effect of this type of attachment was reduction in vibration due to cyclic loading and improving the resolution of the optical measurements (more on optical microscopy will be discussed in section 4.3.2).

Figure 4-1 is a schematic of a build configuration developed to produce a series of standard flat dog-bone samples used in this research. The samples made of Aluminum alloy 7075-T6 which is the same material used earlier in large crack tests (Chapter 3). The geometry of the specimens is shown in Figure 4-1. The dimensions are selected based on ASTM-E466-2007. All dimensions are in millimeter. The edge notch is a half circle with the radius of 0.5 mm.

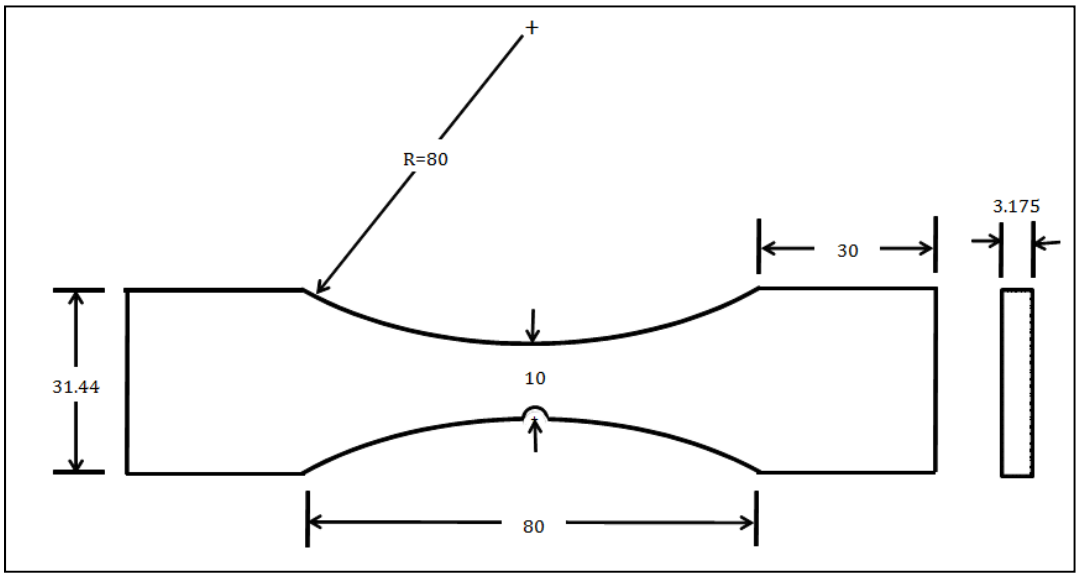

Figure 4-1 Drawing of flat dogbone samples used in fatigue testing, all the dimensions are in mm.

4.3.2 Optical microscopy

Fatigue cracks were monitored online by direct measurement using an optical microscope on the front surface of the samples. The optical measurement system is composed of several components: a high magnification microscope, a video camera attached to the microscope that tracks the behavior of the crack growth for the duration of the fatigue test, a dual arm fiber optic illuminator, a high resolution monitor, an image processing software with the time-lapse photography capability, and a micro-meter scale to calibrate the photographs taken**.** This measurement system allows for detection of small crack lengths, and is sufficient for capturing enough data to correlate observed crack length with the AE signals. Figure 4-2 shows the optical microscopy test set up used for the small crack experiment.

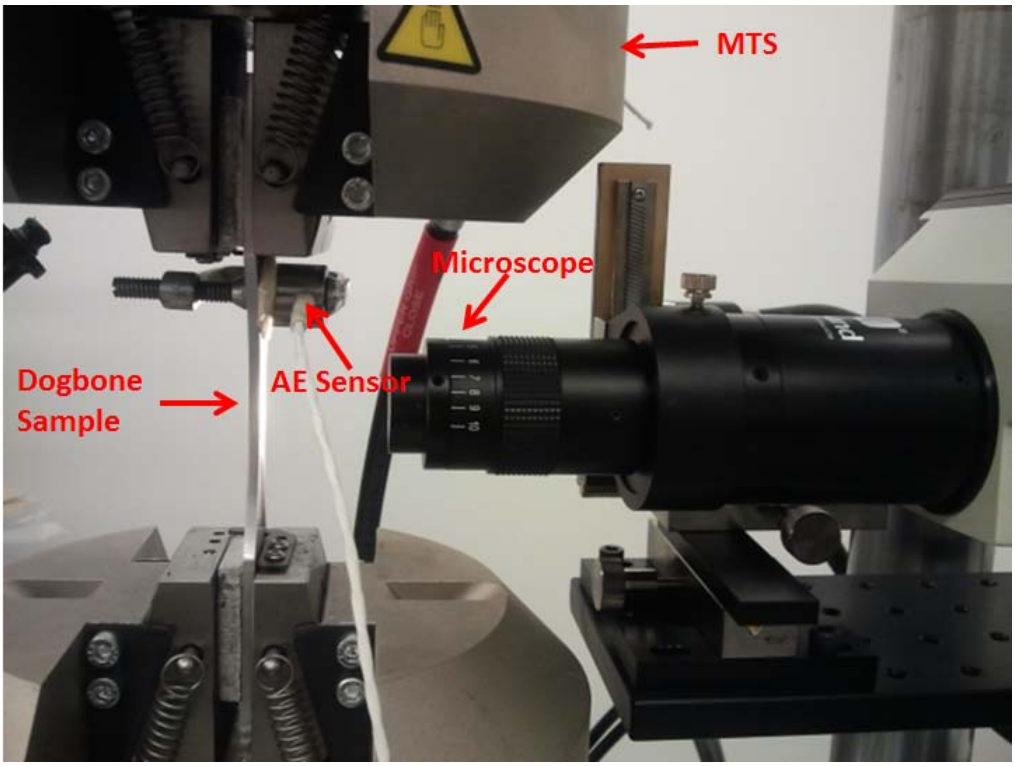

Figure 4-2 Test set up

The assembled optical microscopy unit was focused on the specimen using 100X magnification to observe the specimen notch edge, from which the crack was expected to initiate. A dual arm gooseneck illuminator lighted the target area from both sides, and the camera was used in conjunction with the software to take time-lapse photos of the crack growth. Calibrating the optical system at 100X magnification using a scale ruler and image processing software showed that cracks were could be detected as small as 10 µm. However, the length of practically detected cracks varies depending of the sample movement and consequently the ability of microscope to focus. The smallest crack length practically measurable at 100% of times for all the experiments found to be 0.05 mm (50 µm). As it was mentioned, smaller cracks were detected at some cases, but a crack of 50 µm length was

detectable all the time regardless of the vibration and optical focus. For more information about this measurement refer to sections 4.5.2 to 4.5.5. Crack length was monitored until it exceeds the length of 0.25 mm (250 µm). At this point, sufficient small crack data was collected and crack measurement was terminated. An example of a visual record of the crack length is shown in Figure 4-3.

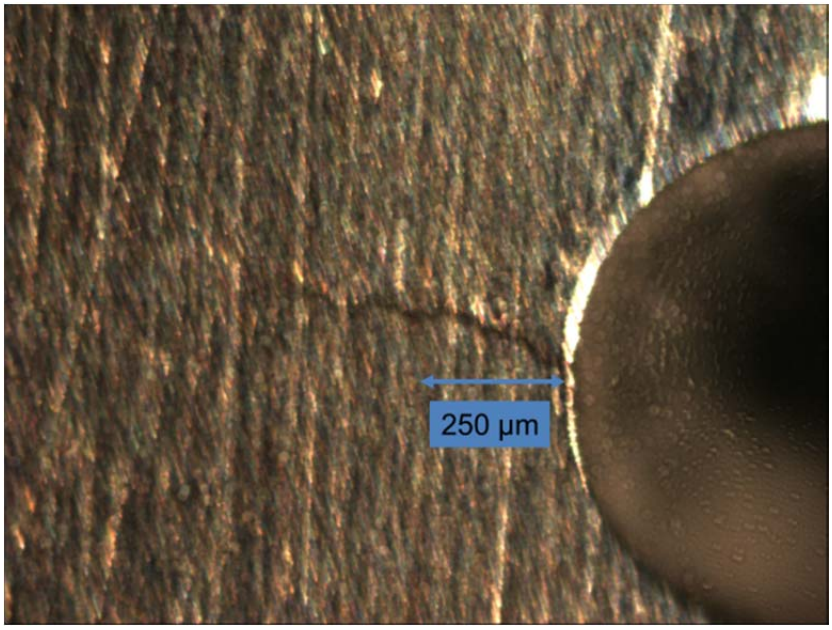

Figure 4-3 Optical crack measurement

4.4 AE fatigue testing

The ultimate goal of this study is to develop an AE-based model for detection of crack initiation and prediction of small crack growth. AE signals may result from a number of possible phenomena including background noise, micro-crack generation or plastic deformation. In order to reduce uncertainties and determine the crack related AE events, applying filtration methods on the captured data was required.

Filtration methods are discussed in the following section, followed by crack measurement method and then AE model development.

In the experimental set up described above, eight fatigue specimens were tested at different loading conditions using both AE and optical microscopy measurement. Table 4-1 lists details of loading parameters for all the tests performed.

Table 4-1. Details of loading parameters for all experiments

Test Reference	*Loading Frequency (Hz)*	*Loading Ratio (R)*	*Force (min-max), KN*
T1	**3**	**0.1**	**0.8 - 8**
T2	**3**	**0.08**	**0.64 - 8**
T3	**3**	**0.1**	**0.8 - 8**
T4	**2**	**0.5**	**6.5 - 13**
T5	**3**	**0.1**	**0.8 - 8**
T6	**2**	**0.3**	**3 - 10**
T7	**2**	**0.5**	**6.5 - 13**
T8	**2**	**0.3**	**3 - 10**

4.5 Data Analysis and Test Results

Based on discussions in chapter 3, background noise (pumps, moving machines, etc.) is difficult to separate from signals. Various de-noising techniques have been discussed in details to capture AE signals due to crack growth for large crack experiments (chapter 3). In the following section de-noising techniques applied to small crack experiments are described.

4.5.1 Noise Reduction

Similar to noise reduction techniques used for large crack experiments (see discussion on de-noising techniques in chapter 3, section 3.4.1), Signals from AE sensor were filtered using a band pass filter (200 kHz- 3 MHz) to eliminate emissions from extraneous sources. Also the AE data taken during loading portion of each cycle were used for data analysis. Additionally, filtered AE events were separated for different percentages of the applied load range and it was determined that for small crack tests, the AE counts occurring within the top 20% of peak load show the closest correlation with crack propagation rates (Gong Z., DuQuesnay D.L., 1998; Morton et al., 1973; Wang et al., 1992). This selection was made based on the recorded AE data from a large group of previous small crack tests on Al-7075. Furthermore, the initial cycles of the recorded data that represent the transient onset response were cut out and the analysis was done using the remaining data. This transient onset response is just the noise of the system at the start of the test and does not carry useful information.

In the small crack growth region, AE count obtained is about an order of magnitude less than that for large cracks in steady state region (Chaswal et al., 2005). Thus, the previously determined threshold of 45dB was too high for this set of experiments. A balance must be made between setting event threshold limit high enough to filter out the majority of the background noise, yet low enough to pick up the beginning of the crack growth. Using a dummy specimen the threshold value was identified to be at 35 dB which was above operational background noise of the machine. This threshold allows for better capturing of crack-related signals. The system was also continuously

set to acquire AE waveforms at a sampling rate of 5 million samples per second. Table 4-2 lists the AE software parameter setting used for small crack tests.

Table 4-2. Parameters of AEWin for small crack tests

Parameter	*Value*	*Unit*
Preamplifier	40	dB (decibels)
Threshold	35	dB (decibels)
Sampling rate	5	MSPS (Million Sample Per Sec.)
Pre-trigger length	100	μs (Micro second)
Hit length	614	μs (Micro second)
High pass analogue filter	200	KHz (Kilo Hertz)
Low-pass analogue filter	3	MHz (Mega Hertz)

4.5.2 Crack Measurement

Eight fatigue specimens under constant amplitude loading (Table 4-1) were monitored using both AE and optical microscopy. The optical microscopy system with time-lapse photography that described in section 4.3.2 was used for monitoring the crack growth. The high volume of captured image were transferred to the image processing toolbox and the pictures taken at crack opening moments were selected for better

measurement of the crack lengths. The lengths of pictured cracks were measured using the Java-based image-processing software (ImageJ).

Crack measurement was started before 50 µm and continued until the crack length larger than 250 µm was observed. At this length the crack exceeds the Navy definition of crack initiation (Papazian et al., 2009) and the crack measurement was terminated. Figure 4-4 Illustrates an example of a sequence of images captured during crack growth of experiment T1. The first image shows observation of a crack as small as 43 µm, and the second picture shows the observation of crack of 51 µm at 3739 cycles.

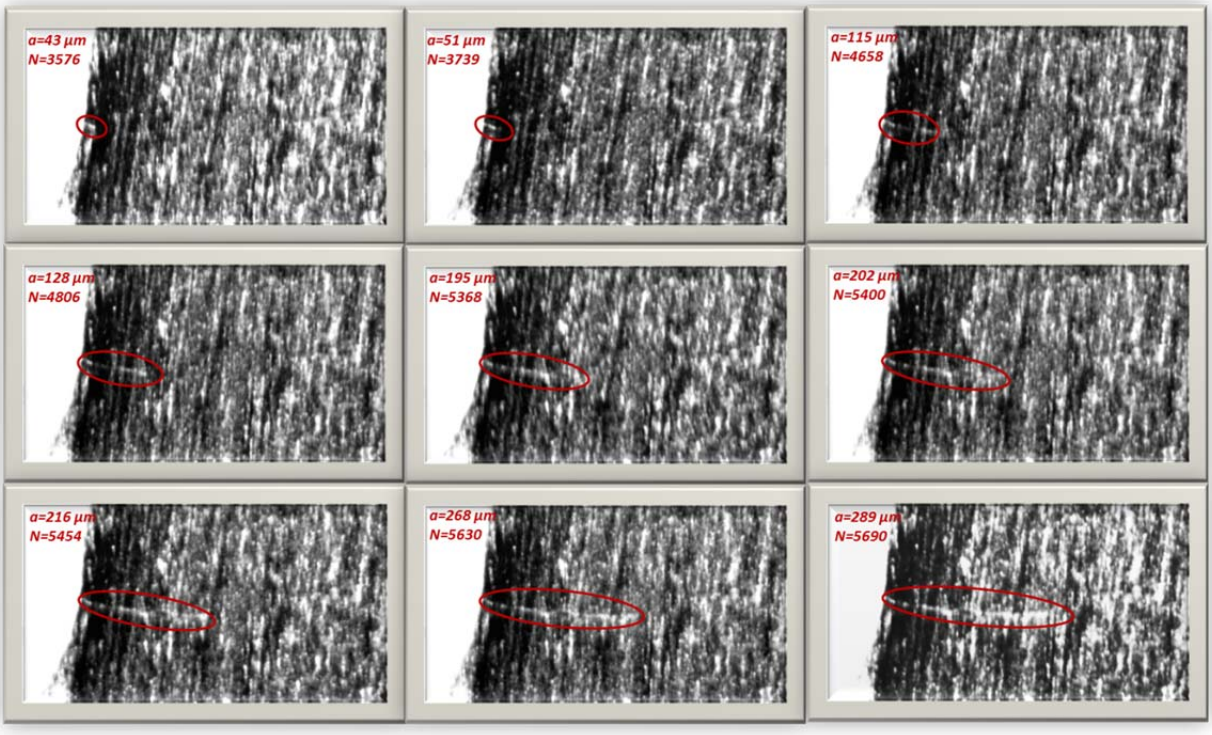

Figure 4-4. A sequence of crack growth images

4.5.3 Uncertainties and Errors

Crack measurement data may be uncertain in nature due to detection uncertainties and measurement errors associated with the optical measurement and sizing process. Detection uncertainties correspond to optical observation of a crack of a given length and will be discussed in this section.

Estimation of crack length and consequently AE-model prediction can be affected by the above-mentioned uncertainties. Therefore, these uncertainties should be characterized properly and should be considered in determining the true crack length for AE model development. In the remainder of this section, two measures of probability of optical crack detection and experimental crack length measurement error are discussed and later used to quantify the uncertainty and validity of the developed AE model.

4.5.4 Probability of detection (POD)

Probability of detection expresses the probability of detecting a crack of a given length and is a common measure to assess the capability of a detection technique. A crack of a given length might be optically detected only at certain percentage of the time (out of the total number of tests) depending on factors such as sample subsurface cracks, vibration, cyclic loadings, optical focus and human error. During the experiments, sometimes a crack was too small to be detected by the optical monitoring system. In this case, the undetected crack could not be followed immediately. Once the crack grew and was spotted, the crack length measurement started. Therefore, a probability of detection (POD) can be used, which is associated

to any defect length. POD can be defined as the probability the optical monitoring will detect the crack of true length *a* and is indicated by POD(*a*).

The POD curve for the used optical crack detection method was obtained by reviewing observation of cracks of various lengths at different experiments and by calculating the ratio of the number of experiments in which the crack of the specified length was detected to the total number of experiments. Generally, POD increases with crack length and eventually attains a maximum value of unity at which all the cracks will be detectable.

There are different methods reported in the literature for POD models. Several models have been suggested in the form of a cumulative distribution function (CDF) of flaw length including logistic and lognormal distribution (Chatterjee & Modarres, 2012) and exponential distribution (Zhang & Mahadevan, 2001).

The POD for various crack lengths was calculated as the ratio of the number of successful detections of a particular crack length over the total number of tests. These POD values are for discrete crack lengths. In order to obtain a continuous POD curve, the POD was estimated by a logistic function for this data. The cumulative distribution function of the log-logistic distribution is (Georgiou, 2006):

$$F(a, m, s) = \frac{\exp \frac{\pi}{\sqrt{3}}\left[\frac{\log a - m}{s}\right]}{1 + \exp \frac{\pi}{\sqrt{3}}\left[\frac{\log a - m}{s}\right]} \tag{4.1}$$

where *m* and *s* are the parameters of the distribution and *a* denotes the crack length.

Figure 4-5 illustrates the POD curve and the fitted logistic cumulative distribution function (CDF). The point estimates of the parameters of the logistic distribution are $m \approx 27$ and $s \approx 9$.

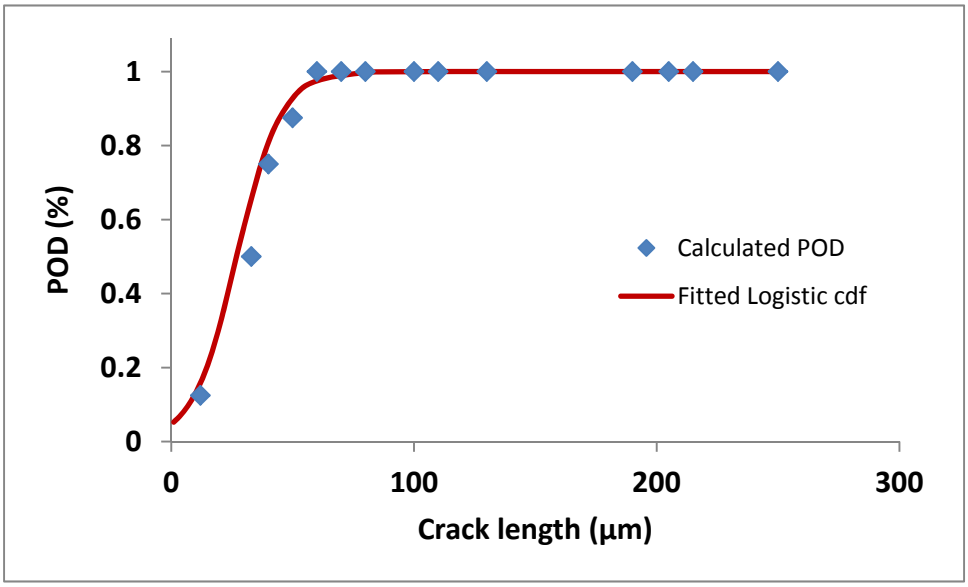

Figure 4-5. Probability of Detection

For the consistency of results and practicality of the approach, a minimum detectability limit was used as the initial crack length. This limit of detectability is defined as the smallest crack length for the applied optical microscopy technique with 100% probability that it will be detected. So, POD(a) would be less than unity for cracks below it. The detectability was selected to be 50 µm. This specified crack length which is smaller than the material's grain diameter, was used as the subjective point of crack initiation in this research. However, the observed data points with smaller crack lengths (a< 50 µm) along with their corresponding PODs (POD<1)

were used in the probabilistic model development. The approach of the probabilistic model development is described in detail in section 4.7.

4.5.5 Crack length measurement error

Due to measurement errors, the experimental results are uncertain and do not exactly represent true values. The precision and accuracy of optical measurement tools, as well as the sizing techniques used to analyze and process the captured pictures of crack growth, contribute to measurement errors. This experimental measurement error is quantified by cross-validating the measurement results with known true crack lengths.

To obtain a good estimation of the true crack lengths, a microscopy technique was used which is described here. When cracked, the specimen was removed from the MTS machine and was transferred to the optiphot microscope in Modern Engineering Material Instructional Lab (MEMIL) at the University of Maryland. This fixed stage microscope is capable of microflex photomicrography with a HFX camera. Using this setting, the final crack length at which the test was stopped was evaluated. An image processing tool (called infinity) was used to capture very high quality pictures of the crack at various magnifications. At each level of magnification, calibration was done by using a scaled ruler. The length of crack was measured later using the captured photographs. The measurements from this optiphot microscope were considered as the true crack lengths and were compared later with the measured crack lengths during online monitoring of the test.

In the next step, the actual crack lengths were compared with the images of the various stages of cracking using photograph taken from the crack at the last cyclic loading of each test. The image processing toolbox of ImageJ was used for this purpose.

The difference between the true length of a crack (a_T) and its experimental measurement (a_M) was calculated and the error was evaluated as:

$$E_a = a_M - a_T \tag{4.2}$$

The relationship between true crack lengths and the experimental measurement is described by some studies (Zhang & Mahadevan, 2001) with a linear function determined by a regression analysis of the form shown in Eq.(4.3). This linear correlation is illustrated in Figure 4-6:

$$a_e = \beta_0 + \beta_1 a_t + \varepsilon_e \tag{4.3}$$

where a_t is the true crack length, a_e is the experimentally measured crack length, β_0 and β_1 are the regression coefficients and ε_e is the residual random error which is assumed to be normally distributed with zero mean value and a standard deviation, σ_e.

$$\varepsilon_e \sim N(0\,, \sigma_e) \tag{4.4}$$

The correlation between the true crack length and the experimental measured crack length was evaluated via Bayesian regression analysis. As a result, the parameters of

the regression model (Eqs (43.) and (4.4)) were estimated using WinBUGS. The results are listed in Table 4-3:

Table 4-3. Estimated parameters of the additive measurement error model

Parameter	Estimated value
β_0	-8.59
β_1	0.984
σ_e	*N(9.96, 2.64)*

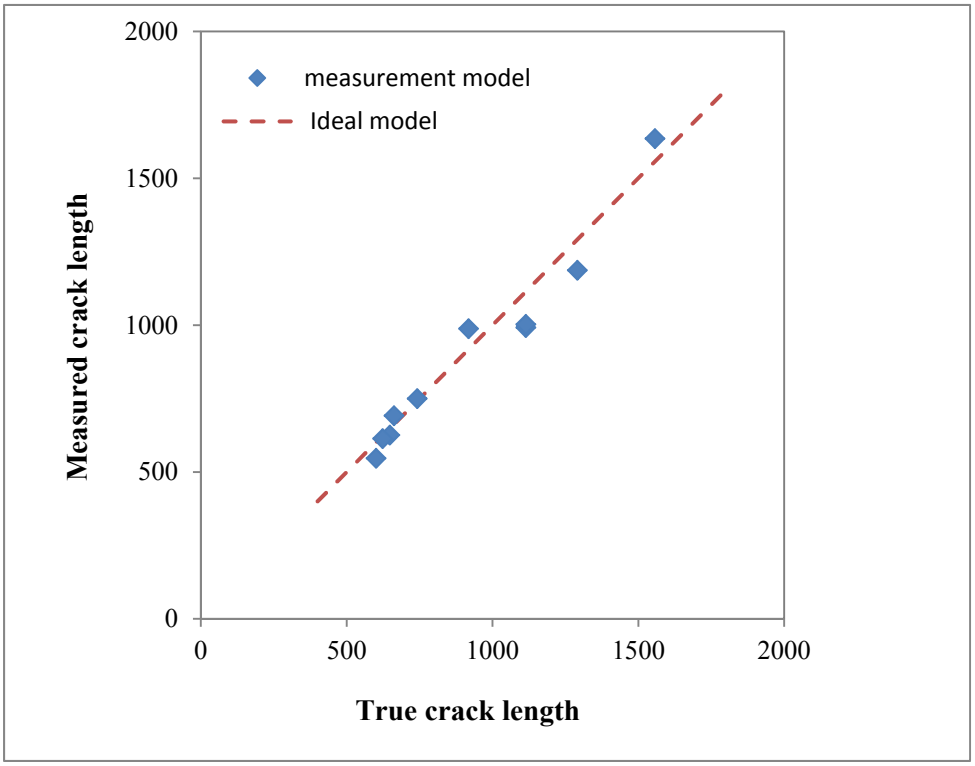

Figure 4-6. Measurement error

To avoid estimation of a negative value for the crack length, which may be caused by the additive error term in Eq. (4.3) for smaller crack lengths, a multiplicative error

model was proposed for estimation of measurement error. Based on the methodology that was outlined in Chapter 3, experimentally measured crack lengths are considered to be estimations and representation of the true crack length, given some error as it is shown in Eq. (4.5):

$$\frac{a_{t,i}}{a_{e,i}} = F_{e,i} \;\; ; \;\; F_e \sim LN(b_e, s_e) \tag{4.5}$$

where $a_{t,i}$ is the true value of crack length, $a_{e,i}$ indicates the experimental measurement results and F_e is the multiplicative error of experiment with respect to true value. The lognormal distribution representing the uncertainty of the multiplicative error has parameters b_e which is the mean of experimental measurement error, as well as s_e which is the standard deviation of the experimental measurement error and both estimated using a Bayesian framework. The summary statistics for the marginal posterior pdf of parameters b_e and s_e as well as the distribution of F_e are presented in Table 4-4. The posterior distributions of the parameters are shown in Figure 4-7.

Table 4-4. Estimated parameters of the multiplicative measurement error model

Parameter	*Mean*	*Standard Deviation*	*2.5%*	*Median*	*97.5%*
be	0.027	0.02678	-0.02497	0.02673	0.08048
se	0.0818	0.0232	0.05062	0.07747	0.1389
Fe	1.031	0.09282	0.8584	1.026	1.236

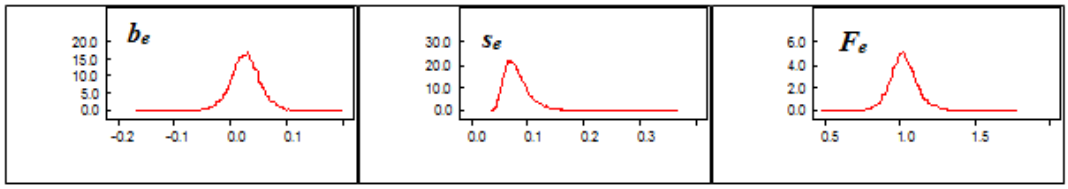

Figure 4-7. Posterior distribution of multiplicative error of experimental measurement

Experimental measurement error bounds can be determined from the 2.5 and 97.5 percentile of the multiplicative error of F_e. The resulting upper bound was calculated as 23% while the lower bound is -14%. These results are presented graphically in Figure 4-8. It can be noticed that there is a very slight shifting (bias) from the true value in the experimental measurement.

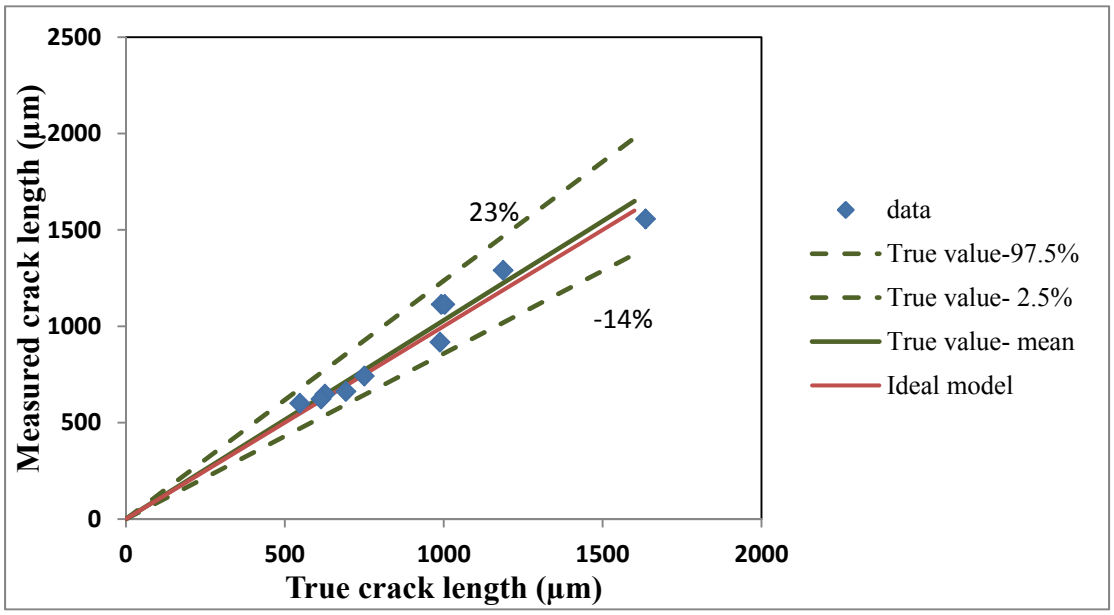

Figure 4-8. Experimental measurement error

The estimated error parameters listed in Table 4-4 were used as the prior knowledge of the crack length measurement error in the Bayesian framework provided for the probabilistic model validation approach. The implemented approach considers both uncertainties in the POD and measurement errors while providing a framework for updating the probability distribution of the model parameters when new data becomes available. For the details of the implemented Bayesian framework refer to section 4.7.2

4.6 AE Results:

Since the primary goal of this study was to develop a method for using acoustic emission to monitor small crack growth, it was necessary to find an empirical relation between AE signals and crack length. In order to do this, recorded AE signals were post-processed and the trends in AE events were evaluated for the duration of test. Any associations between AE features with the damage state were reviewed and based on the observed correlation between AE features and crack length, an empirical relation was developed. The results are discussed in this section and a new approach is proposed to integrate multiple AE features in a predictive model. In order to develop the probabilistic AE-based model, a Bayesian analysis approach was implemented to account for the uncertainties in POD and measurement errors and provide a framework for updating probability distribution of the model parameters using experimental data.

4.6.1 AE Ring-Down Counts

After post processing of the recorded AE signals, the number of cumulative counts was calculated and plotted versus loading cycles. Figure 4-9 illustrates measured cumulative counts for the last experiment (T8 in Table 4-1) at different fatigue loading cycles. A similar trend is observed for the measured crack lengths versus number of cycles at the same time window. An example of such a trend is shown in Figure 4-9.

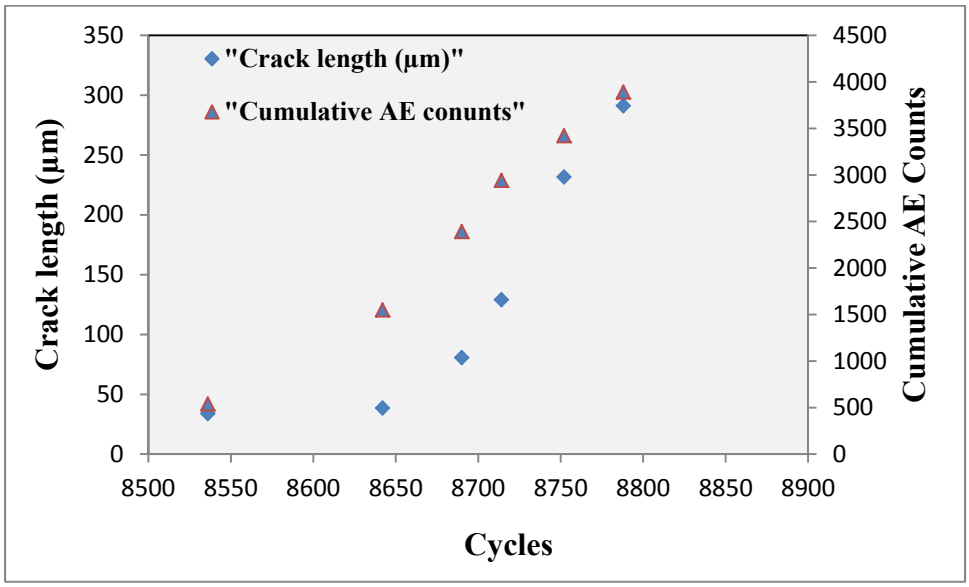

Figure 4-9. Cumulative AE Counts and Crack length

Results show that cumulative AE counts have considerable correlation with the measured crack lengths. As expected, in all experiments performed the calculated AE cumulative counts showed a linear relationship with the length of crack (see Figure 4-10).

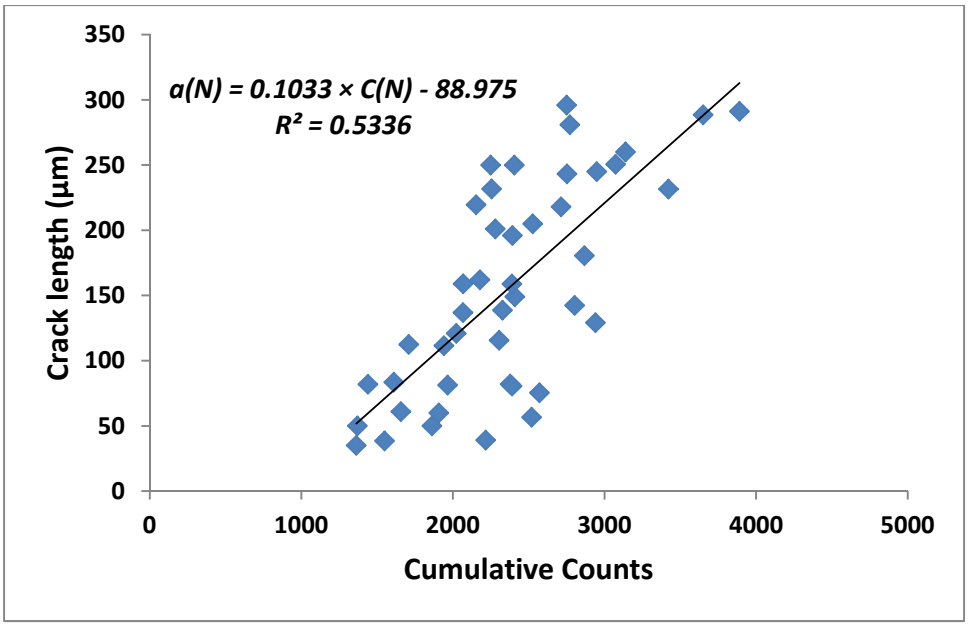

Figure 4-10. Correlation between Cumulative counts and crack length

Figure 4-10 clearly shows that the number of cumulative counts has linear correlation with the crack length. A linear model can be developed based on this relation.

4.6.2 AE Intensity

In order to provide a more effective AE measure of damage, a new approach was developed which employs multiple features of an AE signal and provides a measure for strength of signals.

Generally, it has been suggested that crack related AE signals comprise higher amplitude as well as higher counts (R. K. Miller et al., 2005). Therefore, it can be concluded that the signals with higher amplitudes and higher counts correspond to crack growth rather than noise.

The main idea is that larger cracks produce stronger AE signals and not only the total number of counts, but also with the amplitude level of the AE signal, can quantify this strength. Therefore, estimation of small crack length can be implemented by simultaneous evaluation of these AE features. Based on this idea, a multiplicative correction factor was applied on the acquired counts using the observed amplitude of the signal. This correction factor was defined by the ratio of amplitude over the average or benchmark amplitude of signals.

A new AE index called AE-Intensity was proposed to combine AE counts and amplitude for more effective monitoring of damage state. AE-Intensity is a measure of signal strength and it was shown to have a better correlation with crack lengths. (see Figure 4-11).

The intensity of AE signals is defined by Eq. (4.6):

$$AE\_Intensity: \quad I(t) = C(t) \times \frac{A(t)}{A_0} \tag{4.6}$$

where *C (t)* is the cumulative counts at a specific time *t*, *A (t)* indicates the amplitude of the signal and A_0 is the amplitude threshold which was subjectively selected as *35 dB* for small crack analyses. This selection was made based on the filtration method applied on the data which provides a baseline that any signal amplitude can be compared with.

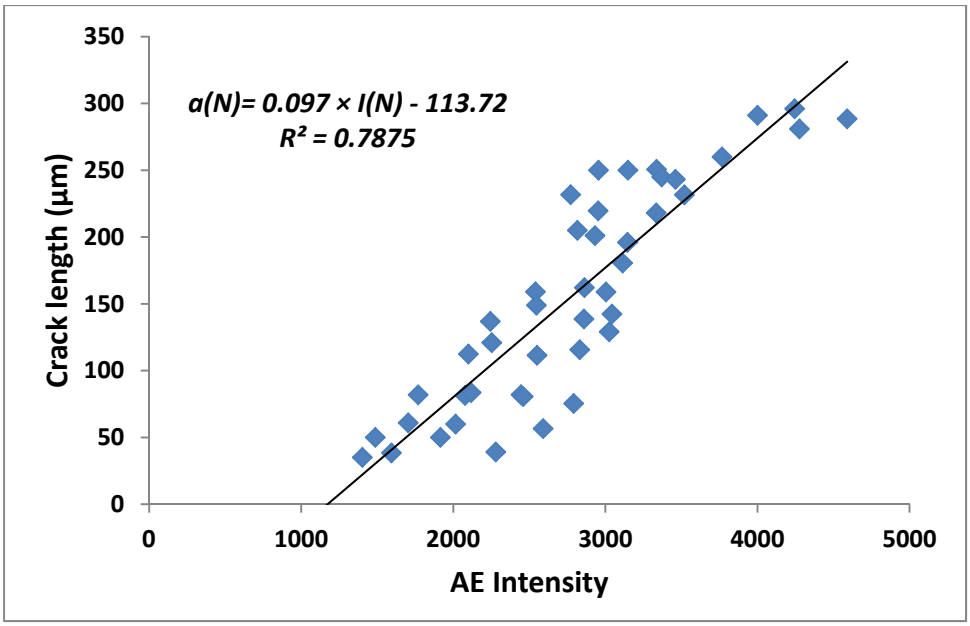

Figure 4-11. Correlation between corrected counts (intensity) and crack length

The linear correlation between crack lengths and AE-Intensity is shown in Figure 4-11. It can be seen that applying the amplitude correction factor to AE count considerably reduces the data scatter in comparison with cumulative counts. Based on the observed relationship, a linear model was proposed which uses AE-intensity as an independent variable and the crack length as dependent variable. The proposed model is introduced in section 4.7.1 by Eq. (4.7).

In the remainder of this chapter, the proposed relationship will be used for probabilistic model development based on experimental data. These are followed by uncertainty analysis and model validation.

4.7 Probabilistic Model Development

The results of the analyzed experimental data were used to develop a probabilistic linear model for the estimation of the small crack length as the dependent variable while AE intensity is considered to be the independent variable. The experimental data obtained in the previous section is divided into two different sets. The first set is used for modeling; the second set is used for estimation of probabilistic error in the model and model validation. The validation data sets were not used in model development (see Table 4-5).

Table 4-5. Separation of data for Model development

	Test Reference	Loading Frequency (Hz)	Loading Ratio (R)	Force (min-max) KN
Modeling	T1	3	0.1	0.8 - 8
	T2	3	0.08	0.64 - 8
	T3	3	0.1	0.8 - 8
Model Validation	T4	2	0.5	6.5 - 13
	T5	3	0.1	0.8 - 8
	T6	2	0.3	3 - 10
	T7	2	0.5	6.5 - 13
	T8	2	0.3	3 - 10

4.7.1 Modeling

According to the observed correlation between AE intensity and crack length, a linear relationship was proposed in the following form:

$$a(N) = \alpha \cdot I(N) + \beta \qquad (4.7)$$

Where *a(N)* indicates the length of small crack after *N* loading cycles, *I(N)* is the calculated AE intensity at cycle *N*, α and β are the unknown model parameters.

In this analysis, true crack lengths were used to evaluate the parameters of the proposed model. To do so, a MATLAB code was developed to implement the measurement uncertainty analysis that was outlined in section 4.5.5.

After the first steps of analyzing the experimental data, results were used to estimate the unknown parameters in the proposed model (Eq. (4.10)) using least square regression analysis. Results are shown in Figure 4-12 and Table 4-6:

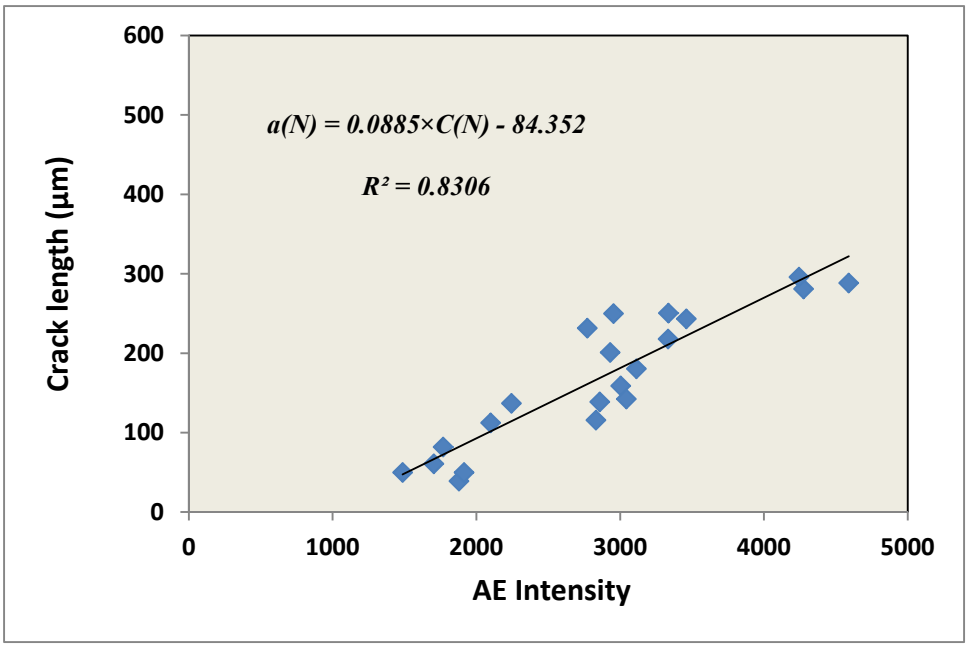

Figure 4-12. Estimation of Model Parameters

Table 4-6. Estimated model parameters

Parameter	*Estimated Value*
α	**0.0885**
β	**-84.352**

4.7.2 Model Validation and Error Estimation

In order to validate the developed AE model, model predictions of small crack length were compared against the validation experimental data set. Similar to the methodology outlined in section 3.8, a multiplicative error approach for model validation was implemented using the validation sets of data to evaluate errors associated with the developed AE-based model and evaluate its prediction uncertainties.

The validation methodology was introduced in Chapter 3 and it is used in this section as well. In the proposed approach (Ontiveros et al., 2010) both model prediction and experimental results are considered to be estimations and representation of the true values, given some error. The multiplicative error of experimental measurement with respect to true value was introduced by Eq (4.5) and the multiplicative error of model prediction with respect to the true value is shown in Eq. (4.11):

$$\frac{a_{t,i}}{a_{m,i}} = F_{m,i}\ ;\ F_m \sim LN(b_m, s_m) \qquad (4.11)$$

where $a_{t,i}$ is the true value, $a_{m,i}$ is the model prediction and F_m is the multiplicative (fractional) error of the model prediction, with respect to the true value. Parameter b_m is the mean (multiplicative) error of the model and s_m is the standard deviation of the error. Accordingly, the multiplicative error of the measurement with respect to the model prediction could be defined similar to Eq. (3.15) as it is shown by Eq. (4.12):

$$\frac{a_{e,i}}{a_{m,i}} = \frac{F_{m,i}}{F_{e,i}} = F_{t,i} \tag{4.12}$$

where $F_{t,}$ is a distribution of the ratio of the experiment and model predictions resulting from multiple iteration of modeling for each experimental data point and can be expressed in the form of Eq. (3.16).

A Bayesian framework was developed to count in the uncertainties associated with POD and crack length measurement error into calculation. The proposed Bayesian probabilistic approach combines prior knowledge of crack length with uncertain experimental data and considers the systematic and random errors and associated uncertainties, to estimate the posterior distribution of crack length. In this approach, the combined effect of POD, measurement errors, and associated uncertainties on measured crack lengths were captured by a likelihood function in the form of Eq. (4.13):

$$L\left(a_{e,i}/a_{m,i}, b_e, s_e \middle| b_m, s_m, m, s\right)$$
$$= \prod_{i=1}^{n} \left(\left(POD\left(a_{e,i}|m,s\right)\right) \left(\frac{1}{\sqrt{2\pi}\left(\frac{a_{e,i}}{a_{m,i}}\right)\sqrt{s_m^2 + s_e^2}} \right) exp\left(\frac{-\left[ln\left(\frac{a_{e,i}}{a_{m,i}}\right) - (b_m - b_e)\right]^2}{2(s_m^2 + s_e^2)} \right) \right) \quad (4.13)$$

where, the POD function is assumed to follow a log-logistic form:

$$POD\left(a_{e,i}|m,s\right) = \frac{\exp \frac{\pi}{\sqrt{3}}\left[\frac{\log\left(a_{e,i}\right) - m}{s}\right]}{1 + \exp \frac{\pi}{\sqrt{3}}\left[\frac{\log\left(a_{e,i}\right) - m}{s}\right]} \quad (4.14)$$

The parameters b_e which is the mean of experimental measurement error, as well as s_e which is the standard deviation of the experimental measurement error were previously estimated in section 4.5.5 and were used in this calculation.

For simplicity the distribution of model predictions were reduced to its mean value and compared one-to-one with the experimental results. The summary statistics for the marginal posterior pdf of parameters b_m and s_m as well as the distribution of F_m are presented in Table 4-7. The posterior distributions of the parameters are shown in Figure 4-13.

Table 4-7. Multiplicative error statistic summary

Parameter	*Mean*	*Standard Deviation*	*2.5%*	*Median*	*97.5%*
b_m	*-0.0575*	*0.02983*	*-0.1159*	*-0.0575*	*0.00021*
s_m	*0.2179*	*0.02346*	*0.1765*	*0.2163*	*0.2676*
F_m	*0.9682*	*0.2188*	*0.6095*	*0.9441*	*1.465*

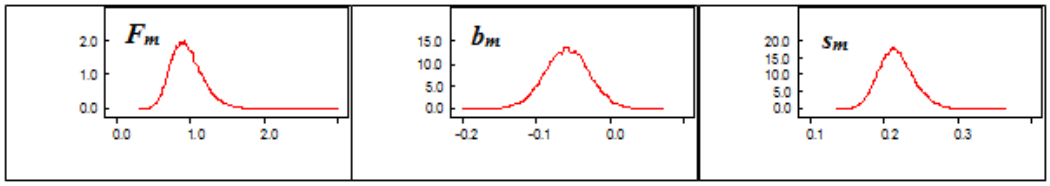

Figure 4-13. Distribution of multiplicative error and it parameters

Model uncertainty bounds for the crack length estimation can be determined from the 2.5 and 97.5 percentile of the multiplicative error of F_m. The resulting upper bound was calculated as 46% while the lower bound is -39%. These results are presented graphically in Figure 4-14. It can be noticed that there is a very slight shifting (bias) from the true value in the results.

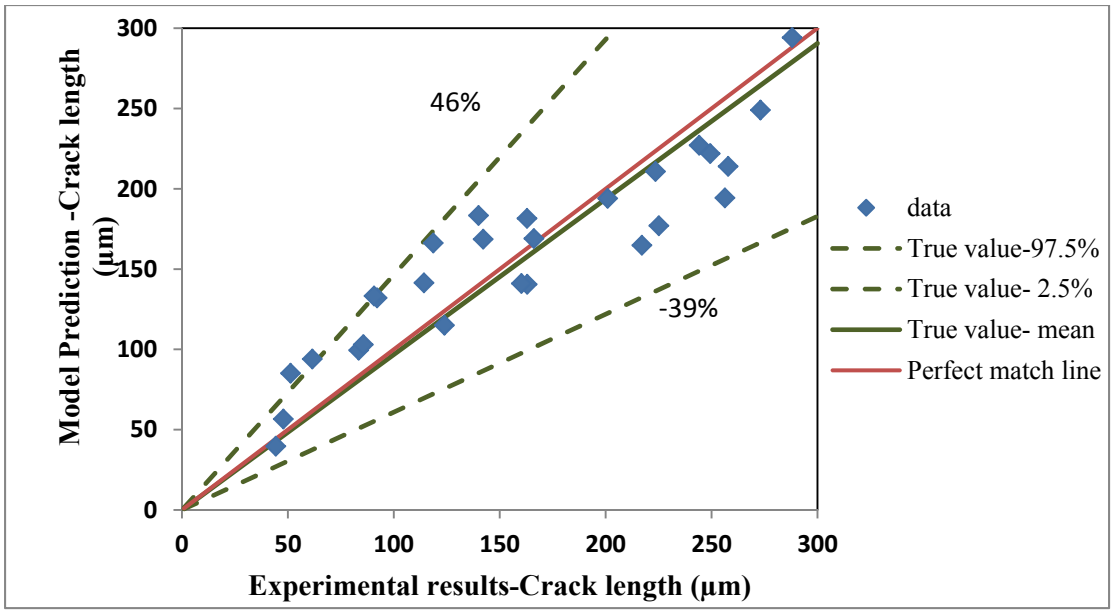

Figure 4-14. Comparison of AE model prediction and experimental results.

Assuming a_m is the model prediction of crack length, the true crack length model prediction then can be estimated by multiplying the distribution of a_m by F_m:

$$a_t = F_m . a_m \tag{4.15}$$

which can be estimated by a lognormal distribution as Eq. (4.18).

$$a_t \sim LN(ln(a_m) + b_m , s_m) \tag{4.16}$$

The model prediction results were modified using the resulted bias distribution. Figure 4-15 illustrates the model prediction uncertainty bounds as well as the modified prediction results. As it can be seen, the developed model slightly over predicts the crack lengths.

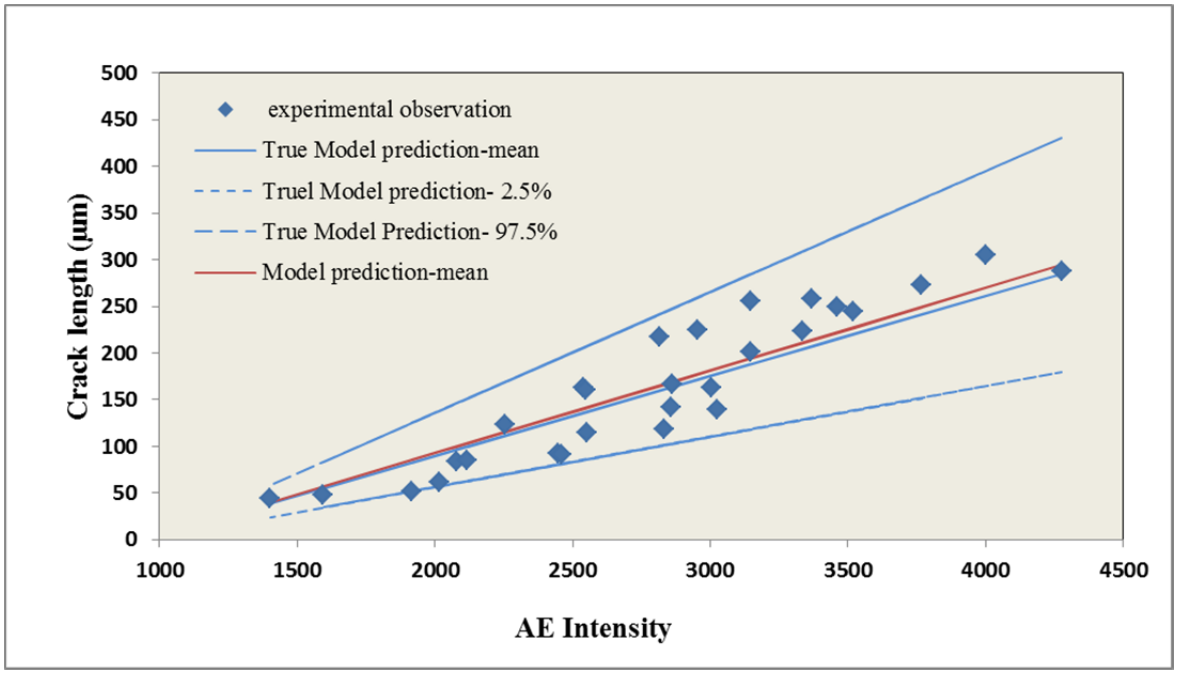

Figure 4-15. Model Prediction with multiplicative error

The validation results in Figure 4-14 show that the developed AE-model allows for crack length estimation given an AE signal. There is a small bias in prediction that can be accounted for with the inclusion of the model error factor, F_m, which allows for an estimation of the true crack lengths. The resulting model can be used to appropriately estimate the true crack length distribution, without a bias.

By using the developed model, for a given value of *I(N)*, distribution of crack length can be estimated. The result of the posterior predictive distribution for *a(N)* as a function of *I(N)* is plotted in Figure 4-15.

The outcome of the proposed model can be used as the evidence in a Bayesian updating process to obtain estimation of crack length at different number of loading cycles and improve prognosis results.

The developed AE model can be effectively used in real time monitoring of small cracks and subsequently can improve processes of structural health management.

5 Chapter Five: Conclusions and Contributions

5.1 Summary

Structural prognosis and health management methods have received significant attention in engineering fields that deal with flaw detection, assessment and monitoring of structures during operation. Structures such as industrial machineries, vehicles and airframes can be subjected to wide range of loading conditions during their service life. Extreme loads may cause initiation of crack and its growth during the life of a component and eventually lead to catastrophic failures. Therefore, a framework for detection and prediction of crack initiation and growth should be developed which will be used in establishing guidelines of safe and cost effective maintenance scheduling. Also, this method should ensure that fatigue cracks will not propagate and fail prior to detection.

The research presented in this dissertation is focused on the structural health monitoring using AE technology as an effective NDT method with potential applications in early detection of crack growth and in-service monitoring of fatigue cracks.

As the first step in the dissertation, a previously proposed relationship between crack growth rate and AE signal features generated during crack growth was modified and validated. This part is focused on the AE model for large crack growth assessment. In order to establish the AE signal feature versus the fatigue crack growth model and study the consistency and accuracy of the model, several standard fatigue experiments

have been performed. These tests were performed using standard test specimens subjected to cyclic loading with different amplitude and frequencies. A Bayesian analysis inference was then used to estimate the parameters of the model and its error. Results indicated that the modified AE crack growth model could be effectively used to predict the crack growth rate distribution at different loading conditions. Additionally, the procedure of probabilistic model development and validation were discussed and uncertainties of the model were investigated. The AE model developed here can be used in real time monitoring of stable fatigue crack growth.

As the second step in this research, a novel methodology for in-situ monitoring of small fatigue crack initiation and growth using AE signal processing technique was introduced. Investigation of uniform cyclic loading tests on Al7075-T6 samples indicated that initiation of cracks smaller than the grain diameter could be identified using statistical analysis of AE signals. Several standard fatigue tests were performed using series of standard flat dog-bone specimens. Acoustic Emission data acquisition was used in conjunction with optical microscopy for online monitoring of crack length. Captured data was used to establish a relation based on the correlation between certain AE signal features generated during crack growth testing and measured crack length. Also, a probabilistic model of fatigue crack length distribution based on the proposed AE signal characteristics was developed.

The obtained experimental data was uncertain in nature due to considerable uncertainties in optical crack detection method and measurement errors associated with the utilized crack sizing technique. To deal with uncertainties, a Bayesian approach was used in this dissertation to consider systematic and random errors in the

model by capturing the combined effect of POD and measurement errors for measured crack lengths. This approach provided a framework for updating the distribution of the model parameters. The updated model can be used for detection of crack initiation as well as prediction of small crack growth in early stages of propagation. Development of this novel AE monitoring technique facilitates early detection of fatigue crack, allows for the original life predictions to be updated and helps to extend the service life of the structure. It should be noted that the implementation of the developed model is limited to Al7075-T6 with the specific geometry of the used samples (see Figure 4-1). The variability of the results has not been reviewed with respect to different materials and different geometries yet.

In the appendix of this dissertation a quantification framework is proposed to evaluate probability of failure of structural integrity using the results of developed AE-based model. The outcome of this method can be used to assess the reliability of structural health by estimating the probability density function of the length of a detected crack at a specified number of cycles and quantifying the probability of failure. Reliability is then assessed by using this quantified failure probability. Finally, remaining lifetime of the structure can be evaluated by using the assessed reliability of the structure after a specified number of stress cycles.

The developed methodology can be utilized for continuous in-service monitoring of structures and has proven to be promising for use in life assessment and remaining useful life prediction of structures subject to fatigue loading. Ultimately, these predictions can be used to define appropriate inspection policies and maintenance schedules.

5.2 Contributions

Major contributions of this research are as follows:

- A novel approach of AE signal processing was proposed and a new characteristic of AE signals was introduced by integrating the non-conventional AE features into a crack growth model.
- The feasibility of detection of crack initiation by using a novel AE waveform de-noising technique has been demonstrated.
- The correlation between small crack growth and the proposed AE characteristic was investigated using the experimental data and the higher performance of this correlation was demonstrated.
- A probabilistic model is developed to represent the relationship between specific AE features and small crack length. Model parameters, along with the associated uncertainties were estimated using experimental data obtained as a part of this research.
- The effect of mean stress and loading frequency on the developed AE crack growth model was investigated by using the obtained experimental data.
- A quantitative approach has been proposed for assessing the reliability of the fatigued structure at a given time, based on the information from the developed AE monitoring system.

Major potential benefits of this research project include:

- Enhance the ability to detect crack initiation and estimate the small crack length distribution in structures under stress.
- Prediction of small crack growth using the developed AE-based NDT approach.
- Real time monitoring and on-time maintenance actions.
- Data driven prognosis to support risk-informed decisions.
- Provide information for SHM.
- Maximize the periodic inspection intervals while minimizing the risk and reduce costly downtimes.

5.3 Suggestions for future research

In this section some topics for potential future work are presented. Future research in this area will be more productive if focused on ideas highlighted below:

- The experimental data used in this research was obtained through standard fatigue tests with constant amplitude loadings. It's recommended to implement a set of experiments to review the effect of random amplitude loading profile on the developed AE model. The main challenge here probably will be to filter out the extraneous noise signals. This becomes even more complicated in the case of variable amplitude loadings.
- The scope of this research does not include addressing challenges of implementing the developed model for different materials and different geometries. It would be desirable to obtain data for samples made of different

geometries and materials and study the applicability of the proposed AE model for some commonly used structures. It should be mentioned that an extensive set of experiments is required to confirm that the AE approach proposed here for small crack growth monitoring is valid for other geometries and materials.

- In this research the location of crack initiation was assumed to be known since the standard specimen was used for experiments. However there are some techniques suggested in the literature to locate the crack using multiple AE sensors. For instance, one of the proposed methods is triangulation which can be used to spot the location of AE source. This method can be applied as an extension of the current work to further enhance the capability of the proposed model for potential industrial applications.

- Finally, in the appendix of this dissertation a quantitative method was proposed for assessing the reliability of the fatigued structure at a specified number of stress cycles, based on information from the developed AE monitoring system. It would be advantageous to integrate this algorithm with the proposed framework. If implemented, it would allow for quantitative assessment of remaining useful life of structures.

6 Appendix

6.1 Overview

In this section, a methodology is proposed for estimating the reliability of structures using results of the proposed AE-based model.

This methodology is based on two of the most commonly used reliability analysis methods; The First Order Reliability Method (FORM) and the Second Order Reliability Method (SORM) .Thus, in this chapter the approach for applying FORM and SORM to evaluate the probability of the structural failure using the estimated crack length resulting from the AE-based model will be discussed.

In this methodology a fatigue failure criterion is associated with the structural component and basically is defined as a limit state function. This function is defined such that it has positive values when the structural health is in the safe region (with respect to the critical crack length) and it has negative values when the structure fails (the existence of a crack of critical length). In the other word, the boundary between two domains is described by the limit state function $g\,(a\,(N),\, a_c) = 0$.

Reliability of a structure is then defined as the probability of the limit state function of random variable *a* being in the safe region $(P\,\{g(a) > 0\})$. Likewise, probability of structural failure is equivalent of the probability of performance function being less than zero $(P\,\{g(a) < 0\})$.Given this definition, the probability of failure after the specified number of stress cycles can be used as a measure to estimate the remaining

useful life of the structural component. For more information about the proposed methodology refer to (Keshtgar, Arcari, Iyyer, Kittur, & Phan, 2012).

6.2 Reliability methods

FORM and SORM are reliability methods which use the joint probability distribution of all uncertain variables to evaluate the probability of failure in a general form of reliability index. The main concept behind these two methods is to calculate the probability of failure by integration of the joint density function over the failure domain.

If the critical crack length is represented by variable a_c and estimated crack length at cycle N is represented by $a(N)$, then the space of state variables is a two-dimensional space as shown in Figure 6-1.

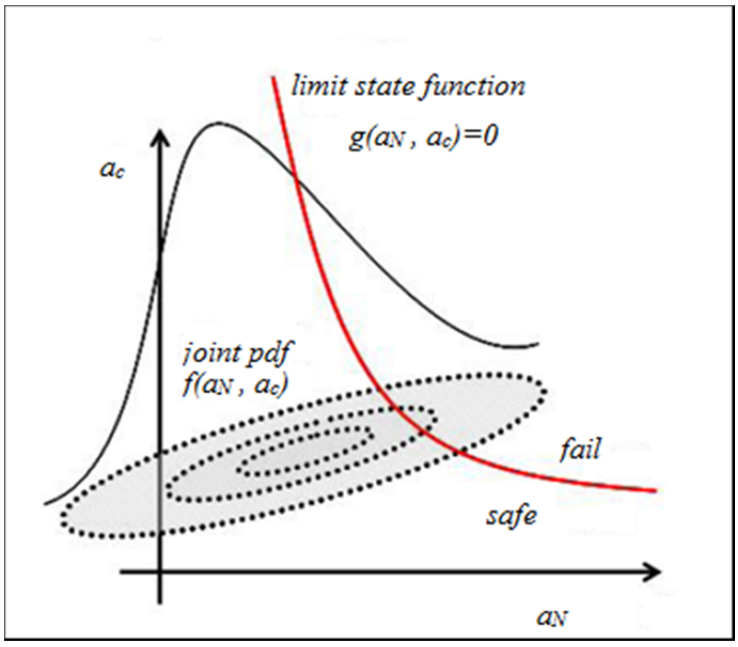

Figure 6-1. Limit state function

In the proposed methodology, reliability is defined based on the probability of failure of the structural integrity. Also, the event of failure is described using the limit state function *g* as a function of estimated crack length *a (N*) and the critical crack length a_c. The limit state function is defined as:

$$g=a_c - a\ (N) \tag{6.1}$$

The probability of failure is the probability that the crack length reaches the failure region (exceed the critical length) at a specified number of loading cycles *(N)* and can be calculated by integration of the joint density function over the failure domain in which $g(a(N),\ a_c) <0$. If the estimated joint *pdf* of *a(N)* is $f_a(a)$, the probability of failure can be calculated with the integral in Equation (6.2)

$$P_f = P[g(a) < 0] = \int_{g(a)<0} f_a(a)da \tag{6.2}$$

And the reliability can be calculated as per Equation (6.3):

$$R = 1 - P_f = P[g(a) > 0] = \int_{g(a)>0} f_a(a)da \tag{6.3}$$

Using FORM and SORM reduces the computational complexity by simplifying the integrand $f_a(a)$. With this simplification and approximation, solutions to Equation (6.2) can be obtained easily. The concept of FORM method is summarized in Figure 6-2. The joint *pdf* , $f_x\ (X)$, is visualized with a two-dimensional case in this figure. The integration boundary $g(X)=0$ is also plotted on X_1-X_2 plane. The integration in Eq. (6.2) is the volume below the surface of the joint *pdf*, $f_x\ (X)$, in the failure region

$g(X) < 0$. In other words, the probability of failure is the volume underneath $f_x(X)$ on the side of failure region $g(X) < 0$ and the reliability is the volume below $f_x(X)$ on the side of safe region $g(X) > 0$.

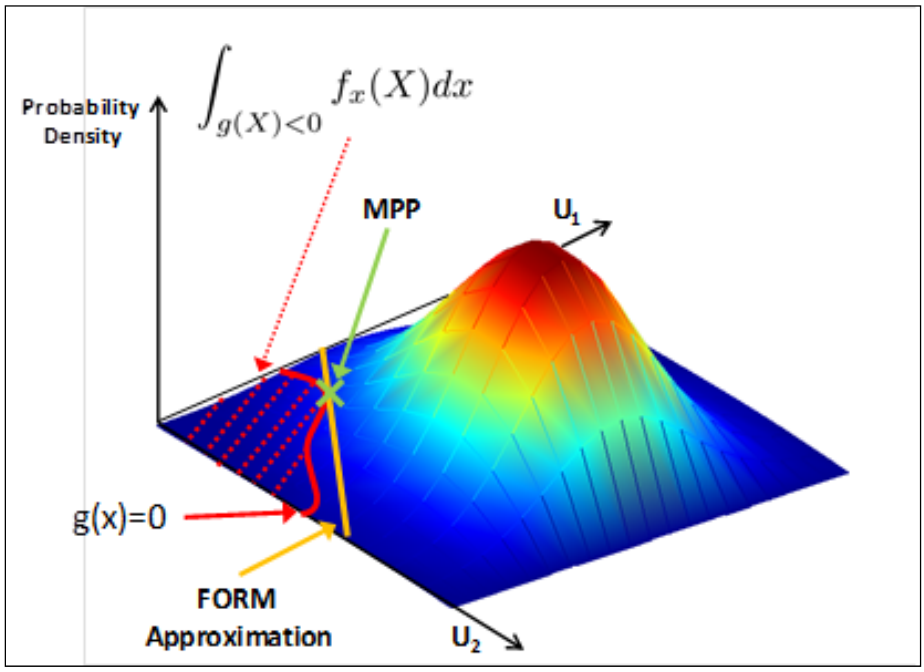

Figure 6-2. Limit state function in transformed space and the FORM approximation

The reliability is measured through a reliability index (β) which is defined as the minimum distance from the origin to the limit state surface $g(U)=0$ as it is shown graphically by the MPP point in Figure 6-2.

After finding the MPP point and the reliability index (β), the probability of failure can be evaluated by:

$$p_f = P\{g(U) < 0\} \approx \Phi(-\beta) \qquad (6.4)$$

and the reliability is calculated by:

$$R = 1 - p_f = 1 - \Phi(-\beta) = \Phi(\beta) \tag{6.5}$$

6.3 Fatigue crack growth model

The developed AE-based model in this research provides a probabilistic estimation of the small crack length. This in conjunction with the proposed methodology can be used to update the reliability estimates and to make decision about the remaining useful life of the structure subject to fatigue.

The applicability of this methodology is further enhanced with the help of the developed fatigue crack growth model which can be applied to small crack region.

The fatigue crack growth model proposed in this research was developed by a research group at the University of Waterloo (Noroozi, Glinka, & Lambert, 2007). This model was applied in developing the software UNIGROW that can be used in modeling both small and large crack growth. The proposed UniGrow fatigue crack growth model is developed based on the elastic-plastic stress-strain response of the material at the crack tip. In this model the stress intensity range (ΔK), is corrected for the presence of the residual stress at the crack tip. The crack growth model was developed in the following form based on total maximum stress intensity factor and total stress intensity range to predict fatigue crack growth under constant amplitude loading (Glinka, Noroozi, & Mikheevskiy, 2007):

$$\frac{da}{dN} = C\left(K_{max,tot}^{p}\Delta K_{tot}^{1-p}\right)^{m} \tag{6.6}$$

It was also shown that equation $\Delta K=K^{0.5}_{max,tot}\,\Delta K^{0.5}_{tot}$ was capable of correlating crack growth data obtained under a wide range of loading ratios with crack growth rates ranging from near threshold rates to high rates (Noroozi et al., 2007). This model can be used for small crack growth evaluation and consequently for estimation of the reliability of structures as described in the next section.

6.4 Proposed Methodology

Based on the discussion above, the following fatigue crack growth model can be used to estimate the crack growth rate.

$$\frac{da}{dN} = C\left(K^{0.5}_{max,tot}\Delta K^{0.5}_{tot}\right)^{m} \tag{6.7}$$

The crack growth rate formulation (Eq. (6.7)) can be integrated to estimate the in-service crack length corresponding to N^{th} stress cycle which is denoted by *a(N)*. The integration domain starts at the number of cycle at which the initial crack was detected and its length was evaluated using the developed AE model. This integration is shown in Eq. (6.8)

$$\int_{a_0}^{a(N)} da = \int_{N_0}^{N} dN.C\left(K^{0.5}_{max,tot}\Delta K^{0.5}_{tot}\right)^{m} \tag{6.8}$$

As discussed earlier, the fatigue failure criterion (the limit state function) of the structure subjected to *N* stress cycles is adopted as:

$$a_c - a\,(N) \leq 0 \qquad (6.9)$$

Where a_c is the critical crack length which is defined as the length of the crack causing failure or a determined crack length beyond which the structure functionality requirement cannot be satisfied. The corresponding failure probability is:

$$P_f = P[g(a(N)) \leq 0] = P[a_c - a\,(N) \leq 0] \qquad (6.10)$$

Note that estimated *pdf* of *a(N)* is a function of all the basic random variables in the crack growth, including *C*, *m* and a_0. The uncertainties associated with these random variables need to be quantified first. Then FORM and SORM will be used to estimate the probability of failure through Eq. (6.10)

The computational procedure of FORM is briefly summarized in Figure 6-3. For a complete overview of the theory and methods of FORM and SORM refer to (Du, 2005).

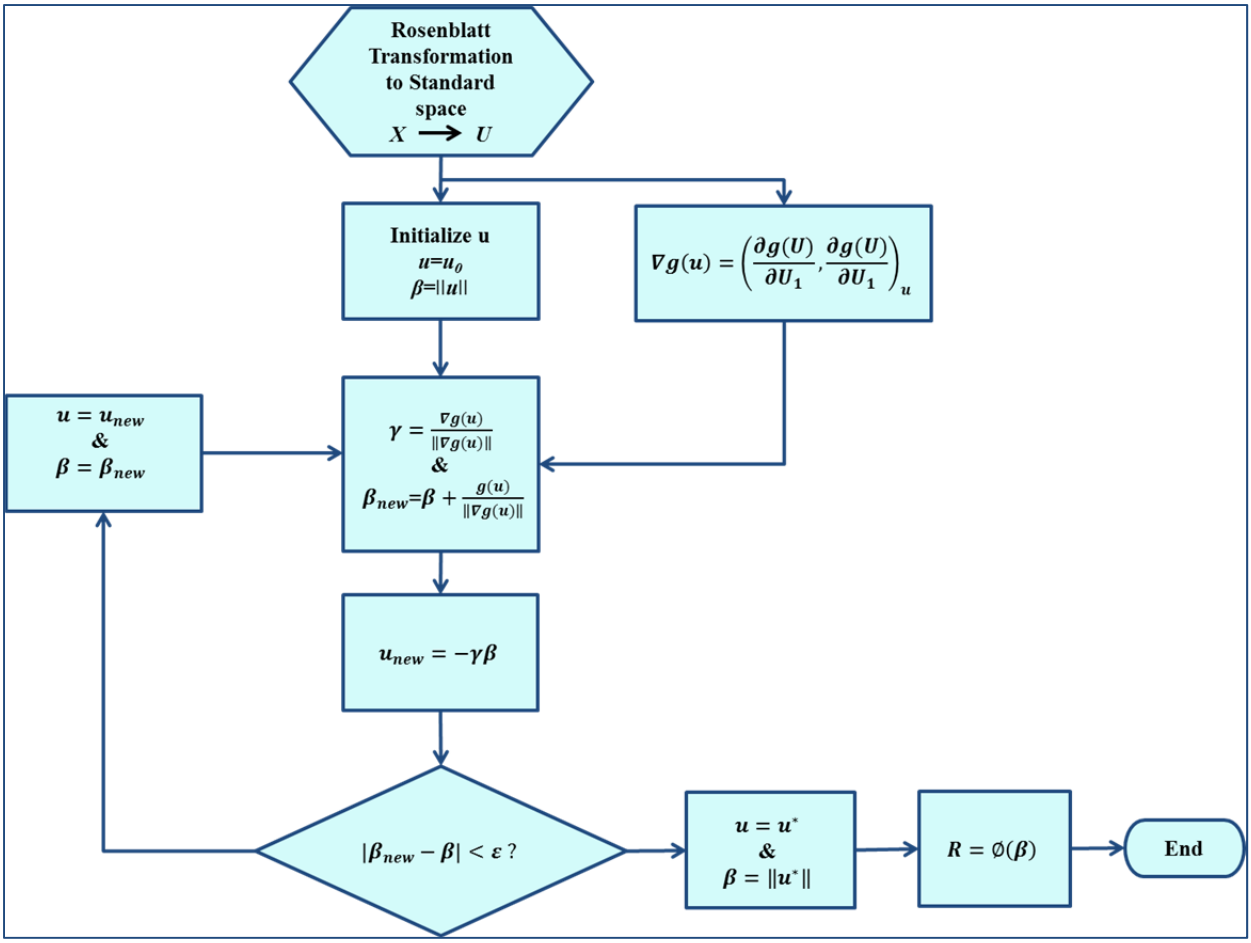

Figure 6-3. FORM algorithm

Generally, SORM is more accurate than FORM as the error committed when approximating with a second order Taylor expansion is smaller than the error committed when approximating with a first order Taylor expansion (Du, 2005).

Variety of solutions are suggested for probability computation using SORM (Y. Lee & Hwang, 2008; Rackwitz, 2001; Zhao & Ono, 1999) A closed form solution is suggested here that was adapted by Lee and Hwang (Y. Lee & Hwang, 2008). This solution counts in the effect of limit state function curvature at MPP. Considering this approach, probability of failure can be obtained using Eq. (6.11):

$$p_f = P\{g(X) < 0\} = \Phi(-\beta) \prod_{i=1}^{n-1} (1 + \beta k_i)^{1/2} \qquad (6.11)$$

where k_i denotes the i-th main curvature of the performance function g(**U**) at the minimum distance point (i.e. MPP) and β is the reliability index calculated by FORM.

To summarize, by using the above-described methodology, reliability of the structure after specified number of cycles can be quantified. Moreover, the remaining useful life of the component can be estimated by implementing this methodology on a range of fatigue loading cycles. (see Keshtgar et al., 2012)

Bibliography

Anderson, T. (1995). *Fracture Mechanics: Fundamentals and Applications*. Boca Raton: Boca CRC Press.

ASTM. (1994). Constant load amplitude fatigue crack growth rate above 10-8 m/cycle (pp. 321–339). American Society for Testing and Materials.

ASTM E466 : Standard practice for coducting force controlled constant amplitude axial fatigue tests of metallic materials. (2012). In *ASTM International* (Vol. i).

Azarkhail, R., & Modarres, M. (2007). A Novel Bayesian Framework for Uncertainty Management in Physics-Based Reliability Models. In *ASME International Mechanical Engineering Congress and Exposition*. Seattle, Washington, USA.

Bannantine, J., Comer, J., & Handrock, J. (1989). *Fundamentals of Metal Fatigue Analysis*. Prentice Hall.

Bassim, M. N., & Liu, C. D. (1994). Detection of the onset of fatigue crack growth in rail steels using Acoustic Emission, *41*(2), 207–214.

Beattie, A. G. (1983). Acoustic emission, principles and instrumentation. *Journal of Acoustic Emission*, *2*, 95–128.

Berkovits, A., & Fang, D. (1995). Study of fatigue crack characteristics by acoustic emission. *Engineering Fracture Mechanics*, *51*(3), 401–416.

Bhattacharya, B., & Ellingwood, B. (1998). Continum damage mechanics analysis of fatigue crack initiation. *Journal of Fatigue*, *20*(9), 631–639.

Biancolini, M., Brutti, C., Paparo, G., & Zanini, a. (2006). Fatigue cracks nucleation on steel, acoustic emission and fractal analysis. *International Journal of Fatigue*, *28*(12), 1820–1825.

Bolstad, W. M. (2007). *Introduction to Baysian Statistics* (second.). Hoboken, NJ: John Wiley and Sons.

Chaswal, V., Sasikala, G., Ray, S. K., Mannan, S. L., & Raj, B. (2005). Fatigue crack growth mechanism in aged 9Cr–1Mo steel: threshold and Paris regimes. *Materials Science and Engineering: A*, *395*(1-2), 251–264.

Chatterjee, K., & Modarres, M. (2012). A probabilistic approach for estimating defect size and density considering detection uncertainties and measurement errors. *Journal of Risk and Reliability*, *227*(1), 28–40.

Ditlevsen, O., & Madsen, H. O. (2007). *Structural Reliability Methods*.

Du, X. (2005). First Order and Second Order Reliability Methods. In *Probabilistic Engineering Design*. Rolla, Missouri: University of Missouri-Rolla.

Eberhardt, E., Stead, D., Stimpson, B., & Read, R. S. (1997). Changes in Acoustic event properties with progressive fracture damage. *International journal of Rock Mech. & Min. Science*, *34*(071), 3–4.

Elforjani, M., & Mba, D. (2009). Natural mechanical degredation measurements in slow speed bearings. *Engineering Failure Analysis*, *16*(1), 521–532.

Ferreria, T., & Rasband, W. (2012). *ImageJ User Guide*. Bethesda, MD, USA.

Forth, S. C., Newman, J. C., & Forman, R. G. (2005). Evaluation of Fatigue Crack Thresholds Using Various Experimental Methods, *2*(6), 1–16.

Fuchs, H. O., & Stephen, R. I. (1980). *Metal fatigue in engineering*. New York: John Wiley and Sons.

Georgiou, G. A. (2006). *Probability of Detection (PoD) curves: Derivation , applications and limitations.*

Gerberich, W. W., & Hartbower, C. E. (1967). Some observations on stress wave eissionas a measure of crack growh. *International journal of fracture mechanics*, *3*, 185–192.

Glinka, G., Noroozi, A., & Mikheevskiy, S. (2007). Unification of notch strain-life and fatigue crack growth theories. In *6th Engineering Integrity Society International Conference on Durability and Fatigue*. Cambridge, UK.

Gong, Z., Nyborg, E. O., & Oommen, G. (1992). Acoustic EmissionMonitoring of Steel Railroad Bridges. *Material Evaluation*, *July*, 883–887.

Gong Z., DuQuesnay D.L., M. S. L. (1998). Measurement and Interpretation of Fatigue Crack Growth in 7075 Aluminum Alloy Using Acoustic Emission Monitoring. *Journal of testing and evaluation*, *26*(6), 567– 574.

Harris, D. O., & Bell, R. L. (1977). The measurement and significance of energy is acoustic emission testing. *Experimental Mechanics*, 347–353.

Iyyer, N., Sarkar, S., Merrill, R., & Phan, N. (2007). Aircraft life management using crack initiation and crack growth models – P-3C Aircraft experience. *International Journal of Fatigue*, *29*(9-11), 1584–1607.

Kappatos, V., & Dermatas, E. (2007). Crack detection in noisy environment including raining conditions. *Aircraft Engineering and Aerospace Technology*, *79*(2), 163–169.

Keshtgar, A., Arcari, A., Iyyer, N., Kittur, M., & Phan, N. (2012). A Reliability Approach for Subcritical Crack Propagation in High Cycle Fatigue. In *15th Australian International Aerospace Congress*. Melborn, Australia.

Kim, K.-B., Yoon, D.-J., Jeong, J.-C., & Lee, S.-S. (2004). Determining the stress intensity factor of a material with an artificial neural network from acoustic emission measurements. *NDT & E International*, *37*(6), 423–429.

Konsztowicz, K. J., & Fontaine, D. (1989). Acoustic emission from crack growth in an advanced zirconia refractory under thermal shock. *Journal of Nondestructive Evaluation*, *8*(1), 1–12.

Kujawski, D., & Ellyin, F. (1992). Crack Initiation and Total Fatigue Life of a Carbon Steel in Vacuum and Air. *Journal of testing and evaluation*, *20*(6), 391–395.

Künkler, B., Düber, O., Köster, P., Krupp, U., Fritzen, C.-P., & Christ, H.-J. (2008). Modelling of short crack propagation – Transition from stage I to stage II. *Engineering Fracture Mechanics*, *75*(3-4), 715–725.

Larsen, J. M., & Allison, J. E. (1992). *SMALL CRACK TEST METHODS*. Philadelphia, PA: American Society for Testing and Materials.

Lee, C. S., Park, C. ., & Chang, Y. W. (1996). Precise Determination of Fatigue Crack Closure in Al Alloys. *Mat. Sci. and Eng.*, *A216*, 131–138.

Lee, Y., & Hwang, D. (2008). A STUDY ON THE TECHNIQUES OF ESTIMATING THE PROBABILITY OF FAILURE. *Journal of Chungcheong mathematical society*, *21*(4).

Lindley, T. C., Palmer, I. G., & Richards, C. E. (1978). Acoustic Emission Monitoring of Fatigue Crack Growth. *Materials Science and Engineering*, *32*, 1–15.

Marder, A. R. (1989). Replication Microscopy Techniques for NDE. In *ASM Handbook : Nondestructive evaluation and quality control*.

Marquez, J. G. M., & Olivares, J. L. (1987). A study of crack initiation and propagation in Ni-Cr thermally sprayed coatings using Acoustic Emission techniques. *Thin Solid Films*, *153*, 243–252.

McDowell, D. L. (1997). Anengineering model for propagationof small cracks in fatigue, *56*(3), 357–377.

Miller, G. A., & Chapman, J. P. (2001). Misunderstanding analysis of covariance. *Journal of Abnormal Psychology*, *110*(1), 40–48.

Miller, R. K., Hill, E. V. K., & Moore, P. O. (2005). *Nondestructive Testing Handbook, Volume 6: acoustic emission Testing* (3rd ed.). ASNT.

Moorthy, V., Jayakumar, T., & Raj, B. (1996). Influence of Microstructure on Acoustic Emission Behavior during Stage 2 Fatigue Crack Growth in Solution Annealed, Thermally Aged and Weld Specimens of AISI Type 316 Stainless Steel. *Mat. Sci. and Eng.*, *A212*, 273–280.

Morton, T. M., Harrington, R. M., & Bjeletich, J. G. (1973). Acoustic Emission of fatigue crack growth. *Engineering Fracture Mechanics*, (5), 691–697.

Noroozi, a, Glinka, G., & Lambert, S. (2007). A study of the stress ratio effects on fatigue crack growth using the unified two-parameter fatigue crack growth driving force. *International Journal of Fatigue*, *29*(9-11), 1616–1633.

Ntzoufras, I. (2009). *Bayesian Modeling Using WinBUGS*. Wiley and Sons.

Ontiveros, V., Cartillier, A., & Modarres, M. (2010). An Integrated Methodology for Assessing Fire Simulation Code Uncertainty, 179–201.

Papazian, J. M., Anagnostou, E. L., Engel, S. J., Hoitsma, D., Madsen, J., Silberstein, R. P., … Whiteside, J. B. (2009). A structural integrity prognosis system. *Engineering Fracture Mechanics*, *76*(5), 620–632.

Paris, P., & Erdogan, F. (1963). A critical analysis of crack propagation laws. Journal of Basic Engineering. *Journal of Basic Engineering*, *85*, 528–84.

Parker, A. (1981). *The mechanics of fracture and fatigue*. London: E & FN spon Ltd.

Pearson, S. (1975). Initiation of fatigue cracks in commercial aluminium alloys and the subsequent propagation of very short cracks. *Engineering Fracture Mechanics*, *7*, 235–247.

Physical Acoustic Corporation. (2007). *AEwin Software User's Manual*. Princeton Junction, NJ.

Rabiei, M. (2011). *A bayesian framework for structural health management using Acoustic Emission monitoring and periodic inspections*.

Rabiei, M., & Modarres, M. (2013). Quantitative methods for structural health management using in situ acoustic emission monitoring. *International Journal of Fatigue*, *49*, 81–89.

Rackwitz, R. (2001). Reliability analysis—a review and some perspectives. *Structural Safety*, *23*(4), 365–395.

Rahman, Z., Ohba, H., Yoshioka, T., & Yamamoto, T. (2009). Incipient damage detection and its propagation monitoring of rolling contact fatigue by acoustic emission. *Tribology International*, *42*(6), 807–815.

Roberts, T. M., & Talebzadeh, M. (2003a). Fatigue life prediction based on crack propagation and acoustic emission count rates. *Journal of Constructional Steel Research*, *59*(6), 679–694.

Roberts, T. M., & Talebzadeh, M. (2003b). Acoustic emission monitoring of fatigue crack propagation. *Journal of Constructional Steel Research*, *59*(6), 695–712.

Shyam, A., Allison, J., & Jones, J. (2005). A small fatigue crack growth relationship and its application to cast aluminum. *Acta Materialia*, *53*(5), 1499–1509.

Smith, F. (1975). Interpretation of adjusted treatment means and regression in analysis of covariance. *Biometrics*, *13*, 282–308.

Talebzadeh, M., & Roberts, T. M. (2001). correlation of crack propagation and AE rates.pdf. Wales: Key Engineering Materials.

Wang, Z. F., Li, J., Ke, W., & Zhu, Z. (1992). Acoustic emission monitoring of fatigue crack closure. *Scripta Metallurgica et Materialia*, *27*(12), 1691–1694.

Williams, J. H., DeLonga, D. M., & Lee, S. S. (1982). Correlations of Acoustic Emission with Fracture Mechanics Parameters in Structural Bridge Steels During Fatigue. *Mat. Eval*, *40*(10), 1184–1189.

Xue, Y., McDowell, D. L., Horstemeyer, M. F., Dale, M. H., & Jordan, J. B. (2007). Microstructure-based multistage fatigue modeling of aluminum alloy 7075-T651. *Engineering Fracture Mechanics*, *74*, 2810–23.

Zhang, R., & Mahadevan, S. (2001). Fatigue reliability analysis using nondestructive inspection. *Jounral of Structural engineering*, *127*(8), 957–965.

Zhao, Y., & Ono, T. (1999). A general procedure for first / second-order reliability method (FORM / SORM). *Structural Safety*, *21*, 95–112.